Shape optimization of two-phase inelastic material with microstructure

Adnan Ibrahimbegović
Ecole Normale Supérieure de Cachan, LMT-Cachan, Cachan, France
Igor Grešovnik
Ecole Normale Supérieure de Cachan, LMT-Cachan, Cachan, France
C3M – Center for Computational Continuum Mechanics, Ljubljana, Slovenia
Damijan Markovič
Ecole Normale Supérieure de Cachan, LMT-Cachan, Cachan, France
Naravoslovnotehniška fakulteta, Univerza v Ljubljani, Ljubljana, Slovenia
Sergiy Melnyk
Ecole Normale Supérieure de Cachan, LMT-Cachan, Cachan, France, and
Tomaž Rodič
Naravoslovnotehniška fakulteta, Univerza v Ljubljani, Ljubljana, Slovenia
C3M – Center for Computational Continuum Mechanics, Ljubljana, Slovenia

Received October 2004
Accepted January 2005

Abstract

Purpose – Proposes a methodology for dealing with the problem of designing a material microstructure the best suitable for a given goal.

Design/methodology/approach – The chosen model problem for the design is a two-phase material, with one phase related to plasticity and another to damage. The design problem is set in terms of shape optimization of the interface between two phases. The solution procedure proposed herein is compatible with the multi-scale interpretation of the inelastic mechanisms characterizing the chosen two-phase material and it is thus capable of providing the optimal form of the material microstructure. The original approach based upon a simultaneous/sequential solution procedure for the coupled mechanics-optimization problem is proposed.

Findings – Several numerical examples show a very satisfying performance of the proposed methodology. The latter can easily be adapted to other choices of design variables.

Originality/value – Confirms that one can thus achieve the optimal design of the nonlinear behavior of a given two-phase material with respect to the goal specified by a cost function, by computing the optimal form of the shape interface between the phases.

Keywords Optimization techniques, Structures, Modelling

Paper type Research paper

The authors gratefully acknowledge the financial supports by the European Commission, through a Marie Curie Fellowship (contract number HPMF-CT-2002-02130), the French Ministry of Research and the Slovene Ministry of Education, Science and Sport. The work of AI was supported by Alexander von Humboldt Foundation.

Engineering Computations:
International Journal for
Computer-Aided Engineering and
Software
Vol. 22 No. 5/6, 2005
pp. 605-645

0264-4401
DOI 10.1108/02644400510603032

1. Introduction

Ever increasing demands to achieve more economical design of a given material result in the need to exploit and analyze its inelastic non-linear behavior. The latter can be formally placed under control by micro-macro models (Ibrahimbegovic and Markovic, 2003), where one goes down to micro-scale in order to obtain a more reliable interpretation of the mechanisms governing the inelastic behavior. This kind of approach opens not only numerous possibilities to obtain a better description of the inelastic behavior of a material than the classical phenomenological models, but also allows one to consider very fine details of the material microstructure and design the one which is the most suitable for a given goal. A number of possibilities can be easily imagined in that respect, from designing a material which will reduce as much as possible the damage in the given zone, thus increasing the durability of the structure, all the way to designing a material which will maximize the damage in a given zone, where it is important to concentrate energy dissipation in a structure.

The design procedure is called upon to guide and accomplish this task. The desired goal is set in terms of the objective cost function (Kleiber *et al.*, 1997), dependent upon the design variables, which can be either geometric or mechanic parameters of the material and its microstructure. The former case, which is of main interest for the work described herein, is more demanding in terms of the solution procedure requirements. Therefore, a novel approach is sought herein with respect to the classical methods (Tortorelli and Michaleris, 1994; Tsay and Arora, 1990) where one separates the optimization problem from the mechanics problem and reduces the communication between the two to the sensitivity computations. The solution procedure for coupled optimization-mechanics problem relies on the method of Lagrange multipliers to bring the two problem ingredients on the same level, which allows much greater flexibility in subsequent solution steps. Another important contribution regarding the solution procedure concerns the phase interface shape representation, which allows a very efficient computation. The details of the solution procedure are presented for the chosen model problem of two-phase material, with one phase as plasticity and another phase as damage. However, the proposed procedure can easily be adapted to other cases of practical interest.

The outline of the paper is as follows. In the next section we briefly review the micro-macro representation of the chosen model problem of two-phase material. A number of practical materials, such as porous metals or concrete, belong to this category. In Section 3 we present the solution procedure for the coupled optimization-mechanics problem. In Section 4 we describe the details of the microstructure representation and the interface shape parameterization. Several numerical examples are presented in Section 5 in order to illustrate a very satisfying performance of the proposed approach. Concluding remarks are stated in Section 6. We also supply an Appendix to explain the details of the proposed approach more clearly in the simple 1D setting.

2. Model problem: micro-macro model of two-phase material

To fix the ideas on multi-scale modeling of inelastic behavior of materials proposed herein, we consider a model problem presented in Figure 1, which is very much representative of standard three-point bending tests, very often used for brittle materials. When trying to interpret the test results in the range of inelastic analysis

and identify more easily the dissipative mechanisms, this would lead us to take into account the details of the material microstructure, and to carry out micro-macro inelastic analysis.

2.1 Micro-macro modeling approach at coupled scales

In targeting the most general application domain, we consider the problem in multiscale analysis of inelastic behavior for the case where the scales remain strongly coupled, imposing the constant communication between the scales. More precisely, in order to more easily identify a particular failure mechanism and its evolution, one is constantly obliged to go down to micro-scale before advancing the computations at the macro scale. The micro-scale can be as small as 1 μm for metals or as large as 1 cm for concrete, so that "micro-scale" terminology should only be interpreted in the relative sense as being much smaller than the macroscale characterizing the structural dimension.

It can happen, such as for large aggregate concrete material, that the ratio between macroscale and micro-scale is not big enough in order to justify the classical scale separation hypothesis, which would allow the computation at the micro-scale to be carried out in advance. Two-scale finite element model can be constructed for this kind of problem as shown in Figure 1, where the finite element representation is provided for each scale. Without loss of generality we assume that all the internal variables are defined only at the micro-scale. The latter implies that the state variables can be written as: displacements at the macroscale, $\mathbf{u}^{\mathrm{M}}$, displacements at the micro-scale, $\mathbf{u}^{\mathrm{m}}$ and the internal variables governing the evolution of inelastic dissipation at the micro-scale, collectively denoted as $\mathbf{v}$. The particular model problem we consider herein pertains to a two-phase material, with the first phase or the matrix represented by a plasticity model and the second phase, represented by a damage model. The set of internal variables therefore consists of plastic strain $\boldsymbol{\varepsilon}^{\mathrm{p}}$, hardening variable for plastic phase ξ^{p}, damage compliance $\mathbf{D}$ and damage hardening variable ξ^{d}. In order to specify the evolution equations of these internal variables we choose the deviatoric plasticity model of the matrix and a simple damage criterion proportional to the spherical stress for the second phase, with a vanishing value of fracture stress in the case when we model inclusions (Ibrahimbegovic *et al.*, 2003). The irreversible nature of the evolution of these internal variables obliges us to carry out an incremental solution procedure, by using one-step time-integration scheme. For a typical time step of one such scheme between t_i and t_{i+1} we can write the central problem of multiscale analysis as follows:

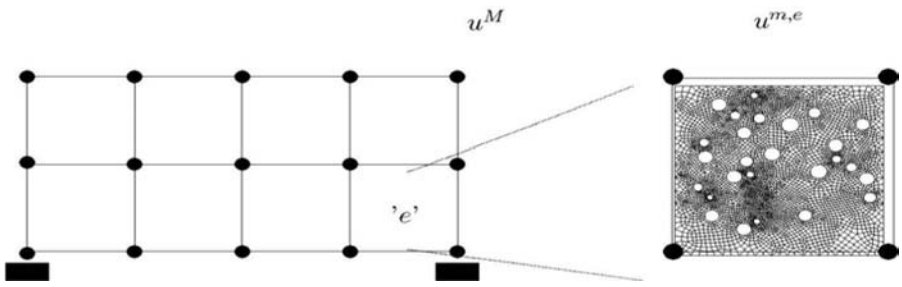

Figure 1.
Micro-macro model of the three-point bending test with macroscale finite element mesh composed of a number of micro-scale finite elements with the exact finite element representation of the material microstructure

Central problem of multiscale analysis

Given the state variables at time t_i,

$$\mathbf{u}_i = \left(\mathbf{u}_i^{\mathrm{M}},\ \mathbf{u}_i^{\mathrm{m}}\right),\ \ \mathbf{v}_i = (\boldsymbol{\varepsilon}^{\mathrm{p}},\ \ \xi^{\mathrm{p}},\ \ \mathbf{D},\ \ \xi^{\mathrm{d}}) \text{ and } \Delta t = t_{i+1} - t_i :$$

Find the corresponding values at time t_{i+1},

$$\mathbf{u}_{i+1} = \left(\mathbf{u}_{i+1}^{\mathrm{M}}, \mathbf{u}_{i+1}^{\mathrm{m}}\right),\ \ \mathbf{v}_{i+1}, \tag{1}$$

such that the weak form of equilibrium equation is satisfied at both scales

$$\mathrm{G}\left(\mathbf{u}_{i+1}^{\mathrm{M}}, \mathrm{u}_{i+1}^{\mathrm{m}}, \mathbf{v}_{i+1}; \mathrm{w}\right) = 0$$

and internal variables evolutions are supplied over time step

$$\mathbf{v}_{i+1} = \mathbf{v}_i + \Delta t[\dot{\gamma}_{i+1}\ \ \partial\Phi/\partial\mathbf{v}_{i+1}],$$

Φbeing the yield/damage criterion, γ the plastic/damage multiplier (Ibrahimbegovic *et al.*, 2003) and w the weighting function.

In the above definition we refer to our recent works (Ibrahimbegovic and Markovic, 2003; Markovic *et al.*, n.d.) for different forms of setting up and solving the equilibrium equations depending upon the chosen scale coupling for either displacement or stress based interface and different microstructure representations. The crucial point in solving these equations pertains to intrinsically different nature of state variables and the displacement field; namely, the weak form features the spatial displacement derivatives and therefore requires the displacement continuity over the boundaries of the micro-scale elements

$$u_i = N_\alpha(\eta_j) u_i^\alpha. \tag{2}$$

This choice results in a large coupled set of equilibrium equations to be solved at the level of each macroscale element, defined as the corresponding assembly of micro-scale elements. On the other hand, no derivatives appear on the internal variables and, for that reason, only independent element-wise values can be used; one typically employs the Gauss quadrature point values, so that the interpolations can formally be defined as

$$\begin{aligned}
&\varepsilon^p = \delta(\eta - \eta^\alpha)\varepsilon_\alpha^p \quad D = \delta(\eta - \eta^\alpha)D_\alpha \\
&\xi^p = \delta(\eta - \eta^\alpha)\xi_\alpha^p \quad \xi^d = \delta(\eta - \eta^\alpha)\xi_\alpha^d \\
&\dot{\varepsilon}^p = \delta(\eta - \eta^\alpha)\dot{\varepsilon}_\alpha^p \quad \dot{D} = \delta(\eta - \eta^\alpha)\dot{D}_\alpha \\
&\dot{\xi}^p = \delta(\eta - \eta^\alpha)\dot{\xi}_\alpha^p \quad \dot{\xi}^d = \delta(\eta - \eta^\alpha)\dot{\xi}_\alpha^d \\
&\dot{\gamma}^p = \delta(\eta - \eta^\alpha)\dot{\gamma}_\alpha^p \quad \dot{\gamma}^d = \delta(\eta - \eta^\alpha)\dot{\gamma}_\alpha^d,
\end{aligned} \tag{3}$$

where $\delta(\cdot)$ denotes the Dirac delta function and η^{α} are abscissas of the chosen Gauss quadrature rule. The central problem is thus transformed in a very large set of independent equations, namely those for internal variable evolution written independently for each Gauss point of micro-scale elements, along with a smaller set of equilibrium equations for each micro-scale element. All the micro-scale elements contributions are assembled and solved for at the level of a single macroscale element, before solving global set of equilibrium equations, which is obtained by the standard finite element assembly procedure of macroscale elements contributions.

The iterative analysis of this kind is driven either by imposed displacement (for displacement based coupling, see Ibrahimbegovic and Markovic, 2003) or imposed stress (for stress based coupling, see Markovic *et al.*, n.d.). Once this analysis has converged we can carry on with a next iterative step at the macroscale. Therefore, the macroscale analysis amounts to formally the same procedure as the standard, single scale finite element analysis, with the only difference related to the manner in which we compute the stiffness matrix and residual vector of these elements, which are available only once the micro-scale computation is carried out. As shown by Markovic *et al.* (2004), the micro-macro solution procedure just described is ideally suited for parallel computations, which allows solving problems with a very large number of unknowns.

2.2 Microstructure representation: exact versus structured mesh representation

The computational framework presented in the previous section relies on the finite element representation of the microstructure in order to explain the failure mechanism. Among a very large number of different possibilities we chose herein a model problem of two-phase material where a plasticity model can describe the inelastic behavior of one phase and the inelastic behavior of the other phase can be represented by a damage model. One can find a number of real materials whose inelastic behavior can be described by a two-phase model of this kind, from the porous metals with damage phase with a vanishing value of damage stress representing the voids, to concrete material where the cement paste behavior is described by a plasticity model and the aggregate behavior is described by a damage model.

Moreover, for the chosen model problem we select a simple microstructure shown in Figure 2(a), where the damage phase occupies a region of circular shape surrounded by the plastic phase spreading to the boundaries of the square cell corresponding to the representative volume element. A slight modification of this microstructure is also considered where the damage phase would occupy a domain of the elliptic shape centered within the square periodic cell, several such cells forming a single macroscale element.

We will first consider the finite element representation of this microstructure, which is referred to as "exact", in the sense that the finite element mesh is exactly adjusted to the domains occupied by each phase, so that every micro-scale finite element corresponds to a sub-domain occupied by only one phase. Any particular micro-scale finite element will thus contain a homogeneous domain, so that the computations can be carried out in completely standard manner.

We can also consider different convenient representations of such a microstructure, which is constructed by using a structured finite element mesh shown in Figure 2(b), where each finite element is of a rectangular shape and the same size, and therefore one micro-scale finite element domain can be shared between both phases. The standard

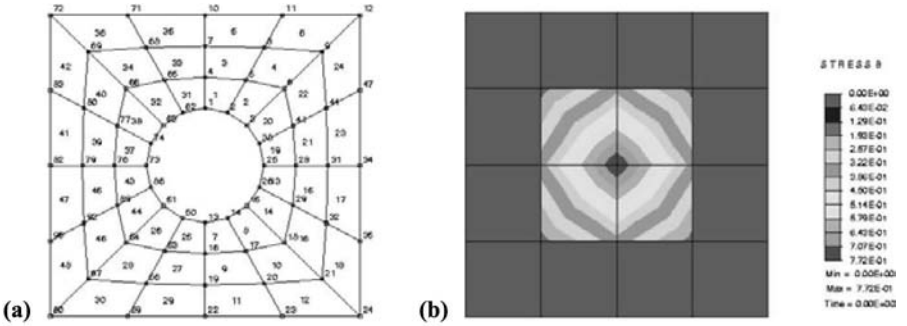

Figure 2.
Finite element representations of the two-phase material microstructure

Notes: (a) exact mesh, where the elements conform with the microstructure, and **(b)** structured mesh, where the mesh is regular and there occur heterogeneities within the elements. The contours in (b) represent the values of the characteristic function $s(x)=0$, if $x \in \Omega^p$ and $s(x)=1$, if $x \in \Omega^d$, where Ω^p and Ω^d denote the plastic phase (matrix) and damage phase (or void) domain, respectively

computational procedure for each micro-scale finite element can no longer be used to guarantee the sufficient result accuracy and one has to consider different enhancements. Three different possibilities exist, such as:

(1) Gauss numerical point (GNP) filtering (Wriggers and Zohdi, 2001);

(2) incompatible mode representation (Ibrahimbegovic and Markovic, 2003); and

(3) stress based representation (Markovic *et al.*, n.d.).

The accuracy of these structured mesh representations can be brought to the level the exact microstructure representation, only with the last two.

3. Solution procedure of coupled analysis and optimisation

3.1 Lagrange multiplier method basis for coupled solution procedure

The classical optimization procedure, pertaining to the design of engineering structures, can be extended to the presented class of problems in order to provide the optimal design of a composite material. The notion of desired, optimal performance is more precisely specified in mathematics language in terms of the cost or objective function. This cost function is specified in terms of so-called design variables, which are used to define either geometric and/or material properties of the structure in its initial configuration (Kleiber *et al.*, 1997).

Some examples of cost functions for structures involve weight, strength or amplitude of the stress field. Any of these criteria can be exploited in designing the optimal behavior of a particular composite material, but one can also devise a number of new, less frequently used choices for the cost function that would specify better the desired inelastic behavior of a given material. One such example is related to a very important issue of material durability, where one would seek the composite material arrangement that would limit inelastic behavior to a minimum. Another example of this kind concerns the materials used in vibration isolation system in order to reduce the structural damage in structures, where one would seek to maximize the damage in the isolation layers. For either of these cases a very suitable choice for the cost function

is the inelastic dissipation. For a two-phase model material we consider herein, the total dissipation is the sum of the plastic and damage dissipation, which can be expressed according to (Ibrahimbegovic *et al.*, 2003)

$$\dot{D}^d + \dot{D}^p = \frac{1}{2}\boldsymbol{\sigma}\dot{D}\boldsymbol{\sigma} + q^d\dot{\xi}^d + \boldsymbol{\sigma}\dot{\varepsilon}^p + q^p\dot{\xi}^p. \tag{4}$$

where the first two terms express the damage and the last two the plastic dissipation at each point with the known values of the internal variables and their evolution. In equation (4), $\boldsymbol{\sigma}$ is the stress tensor, whereas q^d and q^p are stress-like variables that describe hardening effects for damage and plasticity phase, respectively.

The design problem in the classical sense can then be interpreted as the constrained minimization of cost function $j(\cdot)$ in terms of design variables $\mathbf{p}$, which can be written as follows:

$$\mathbf{p} = \left\{\mathbf{p}^*; \min_{G(\ldots)=0}\ j(\mathbf{p}, \cdot)\right\}, \tag{5}$$

where the constraints pertain to the weak form of the equations governing the equilibrium at both macro- and micro-scale, as well as the evolution equations of the internal variables, as specified in the previous section. The cost function can be defined as minimizing the dissipation (when we want to ensure durability) or minimizing the negative of dissipation (when we want to ensure concentration of inelastic behavior in an isolation device) in a given region of the structure throughout the loading time history, which can be written as

$$j(\mathbf{p}, \mathbf{u}(\mathbf{p}), \mathbf{v}(\mathbf{p})) = \int_0^T \int_\Omega (\dot{D}^p + \dot{D}^d)\mathrm{d}\Omega\,\mathrm{d}t \tag{6}$$

Rather than adopting the classical formulation of the optimization problem (Kleiber *et al.*, 1997), we follow the previous work by Ibrahimbegovic and Knopf-Lenoir (2003) or Ibrahimbegovic *et al.* (2004) to make use of the Lagrange multiplier technique to eliminate the constraint in equation (5). In this process we bring the mechanics equations at the same level as the cost function. In other words, the state variables to perform mechanics analysis are also brought to the same level as the design variables and, contrary to the statement in equation (6), the state variables can now be considered as independent from the design variables. The latter implies that the solution procedure can be carried out in any chosen order, and it can thus become quite different from the classical optimization computation.

The coupled analysis and optimization problem of this kind can be formulated by introducing the Lagrangian functional

$$\min_{d,u,V} \max_\lambda L(p, u, V, \lambda) = J(p, u, V) + G(p, u, V; \lambda), \tag{7}$$

where λ is the set of the Lagrange multipliers enforcing different constraints in micro-macro mechanics model, containing both the local multipliers λ^v for internal variables and global ones λ^{eq} for displacement field. The second term on the right hand side in equation (7) takes the same form as the weak form of the governing equilibrium and evolution equations, with the corresponding Lagrange multiplier replacing the variations of the state variables.

The Kuhn-Tucker optimality conditions corresponding to the Lagrangian functional in equation (7) can be written as follows:

Variation with respect to the Lagrange multipliers returns the corresponding macroscale and micro-scale equilibrium and internal variable evolution equations of the problem:

$$\frac{\partial L}{\partial \lambda} = G = 0 \tag{8}$$

Variation with respect to the internal variables provides a set of equations to solve at each Gauss point:

$$\frac{\partial L}{\partial V} = \frac{\partial J}{\partial V} + \lambda^{\mathrm{V}} \frac{\partial G}{\partial V} = 0 \tag{9}$$

Variation with respect to the displacement field features the tangent operator:

$$\frac{\partial L}{\partial u} = \frac{\partial J}{\partial u} + \lambda^{eq} \frac{\partial G}{\partial u} = 0 \tag{10}$$

Variation with respect to the design variables will typically couple all the variables and lead to the most elaborate equation:

$$\frac{\partial L}{\partial p} = \frac{\partial J}{\partial p} + \lambda \frac{\partial G}{\partial p} = 0 \tag{11}$$

One can further simplify these equations in view of providing their discrete approximation. In particular, the choice of discrete approximation of the Lagrange multipliers is equivalent to the discrete approximations chosen for the variations of corresponding state variables, which is being replaced by the corresponding Lagrange multipliers in the Lagrangian functional in equation (7). For example, the inter-element continuity requirement at the micro-scale is imposed on the Lagrange multipliers for equilibrium equations with

$$\lambda_i^{eq} = \sum_{\beta=1}^{2} N_\beta(\eta_i) \lambda_{i,\beta}^{eq}. \tag{12}$$

Similarly, the discrete approximations of the Lagrange multipliers for internal variables are picked up so as to reduce their contributions to Gauss quadrature points only with

$$\begin{aligned} &\lambda^{\Phi^p} = \delta(\eta - \eta^\alpha)\lambda_\alpha^{\Phi^p}; \quad \lambda^{\Phi^d} = \delta(\eta - \eta^\alpha)\lambda_\alpha^{\Phi^d}; \quad \lambda^{\varepsilon^p} = \delta(\eta - \eta^\alpha)\lambda_\alpha^{\varepsilon^p} \\ &\lambda^{D} = \delta(\eta - \eta^\alpha)\lambda_\alpha^{D}; \quad \lambda^{\xi^p} = \delta(\eta - \eta^\alpha)\lambda_\alpha^{\xi^p}; \quad \lambda_\alpha^{\xi^d} = \delta(\eta - \eta^\alpha)\lambda_{\alpha,n}^{\xi^d} \end{aligned} \tag{13}$$

The Lagrangian functional in equation (7) can then be written to indicate explicitly all the independent variables

$$L = L(p, \varepsilon(u), \varepsilon^p, \xi^p, D, \xi^d, \dot{\varepsilon}^p, \dot{\xi}^p, \dot{\gamma}^p, \dot{D}, \dot{\xi}^d, \dot{\gamma}^d; \lambda). \tag{14}$$

This number of the independent variables can further be reduced by taking into account the finite difference approximations for time derivatives of all the internal variables, which is in accordance with the backward Euler time integration of the corresponding evolution equations on internal variables in the central problem in equation (1)

$$\begin{aligned} \dot{\varepsilon}^{p}_{\alpha,n} &= \frac{\varepsilon^{p}_{\alpha,n} - \varepsilon^{p}_{\alpha,n-1}}{t_n - t_{n-1}} \quad \dot{D}_{\alpha,n} = \frac{D_{\alpha,n} - D_{\alpha,n-1}}{t_n - t_{n-1}} \\ \dot{\xi}^{p}_{\alpha,n} &= \frac{\xi^{p}_{\alpha,n} - \xi^{p}_{\alpha,n-1}}{t_n - t_{n-1}} \quad \dot{\xi}^{d}_{\alpha,n} = \frac{\xi^{d}_{\alpha,n} - \xi^{d}_{\alpha,n-1}}{t_n - t_{n-1}} \end{aligned} \tag{15}$$

By making use of these finite difference approximations we can reduce the number of Kuhn-Tucker optimality conditions by four; more precisely, by employing the chain rule in order to express the variations with respect to internal variable rates with respect to the variations of the internal variables, the result in equation (9) can be restated as

$$\begin{aligned} &\left(\frac{\partial L}{\partial \varepsilon^{p}} + \frac{1}{\Delta t_n}\frac{\partial L}{\partial \dot{\varepsilon}^{p}}\right)\delta\varepsilon^{p} = 0; \quad \left(\frac{\partial L}{\partial D} + \frac{1}{\Delta t_n}\frac{\partial L}{\partial \dot{D}^{p}}\right)\delta D = 0 \\ &\left(\frac{\partial L}{\partial \xi^{p}} + \frac{1}{\Delta t_n}\frac{\partial L}{\partial \dot{\xi}^{p}}\right)\delta\xi^{p} = 0; \quad \left(\frac{\partial L}{\partial \xi^{d}} + \frac{1}{\Delta t_n}\frac{\partial L}{\partial \dot{\xi}^{d}}\right)\delta\xi^{d} = 0 \end{aligned} \tag{16}$$

Having thus reduced the number of unknowns and their domain of definition to a minimum needed, the solution procedure can be started. The preferred order we choose is to first solve for the all internal variable increments at all Gauss points from equation (16) above to obtain ΔV^{d} and ΔV^{p}; this kind of computation also implies solving for the stress plastic and/or damage admissibility conditions $\Phi^{p} = 0$ and $\Phi^{d} = 0$. Solving equation (8) for micro-scale and macroscale displacement incremental fields Δu is carried out next, by using the multiscale solution procedure, as described in the previous section.

The optimization loop starts by solving from equation (10) for all Lagrange multipliers $\Delta\lambda^{eq}$, $\Delta\lambda^{V^{d}}$ and $\Delta\lambda^{V^{p}}$. The latter reduces to a linear problem, as the consequence of the choice of the dual formulation in equation (7). The last solution concerns the new increment of the design variables Δp computed from equation (11). For clarity, we provide in the Appendix all the details of this solution procedure for a 1D case of the optimal design of composite truss-bar with one part built of plastic and the rest of damage material.

3.2 Software architecture for coupling of analysis and optimization

The entire solution procedure is naturally divided into two parts. The inner part consists of solution of the mechanical problem and calculation of the objective and constraint functions for given values of the design parameters, and the outer part consists of solving for optimal design variables by using the solution of the inner problem. The multi-scale solution procedure for the mechanical problem has been implemented in the finite element environment "FEAP" (Taylor, 2004). The procedure has been parallelized in such a way that the problems at the

microscopic level (each corresponding to one macro element) are solved simultaneously over a heterogeneous network of computers (Markovic *et al.*, 2004). This speeds up the numerical solution of the mechanical problem enough that performing optimization on top of it becomes feasible.

Solution of outer part was performed by the optimization program "Inverse" (Grešovnik, 2000; Rodič and Gresovnik, 1998; Grešovnik, n.d.). This program has been designed for linking optimization algorithms and other tools through a suitable interface with numerical analysis environments. It is built around interpreting language that enables flexible and transparent access to the implemented functionality for setting up the solution schemes for specific problems. The concept has been confirmed on a large variety of problems, including many in the field of metal forming (Grešovnik, 2000; Grešovnik and Rodič, 1999, 2003) where numerical analyses involve highly non-linear and path dependent material behavior, large deformation, multi-body contact interaction and consequently large number of degrees of freedom.

"Inverse" carries out the optimization algorithm that solves the outer problem, controls the solution of the inner mechanical problem and takes care of connection between these two parts. Prior to calculation of the objective and constraint functions, input for mechanical analysis is prepared according to the current values of design parameters. In the phase interface optimization problem we would like to solve herein, the latter corresponds to generation of the finite element mesh that is used for each macro element. The mesh for a single cell or a single macroscale element is generated first on the basis of a template mesh corresponding to a circular inclusion, by transforming node co-ordinates as described in detail in the next section. Subsequently, we assume the periodic microstructure, which allows us to combine several periodic cells in order to obtain the complete macroscale finite element mesh. The latter is stored to a file in the prescribed format where it can be accessed by the FEAP micro-macro analysis. This procedure is graphically illustrated in Figure 3.

In the optimization phase, the calculation of the response functions includes solution of the mechanical problems and integration of the relevant quantities, which is performed in "FEAP". These results are passed to "Inverse" through arguments of the analysis procedure, which was prepared in "FEAP" for the complete calculation of the response functions of the optimization problem. Although the interfaces with simulation codes usually involve more sophisticated control over program flow and internal data (Grešovnik, 2000), this kind of interfacing appeared the quickest way to solve our problem, largely due to openness and extensibility of "FEAP". Main advantages of linking "Inverse" with "FEAP" and using it for optimization are more transparent definition of the problem, simple and systematic application of modifications to the original problem, and accessibility of already incorporated utilities. These include different optimization algorithms, tabulating utilities, automatic recording of algorithmic progress and other actions, debugging utilities, automatic numerical differentiation, and an useful bypass utility for avoiding memory heaping problems that may be difficult to avoid when a stand-alone numerical analysis software is arranged for iterative execution.

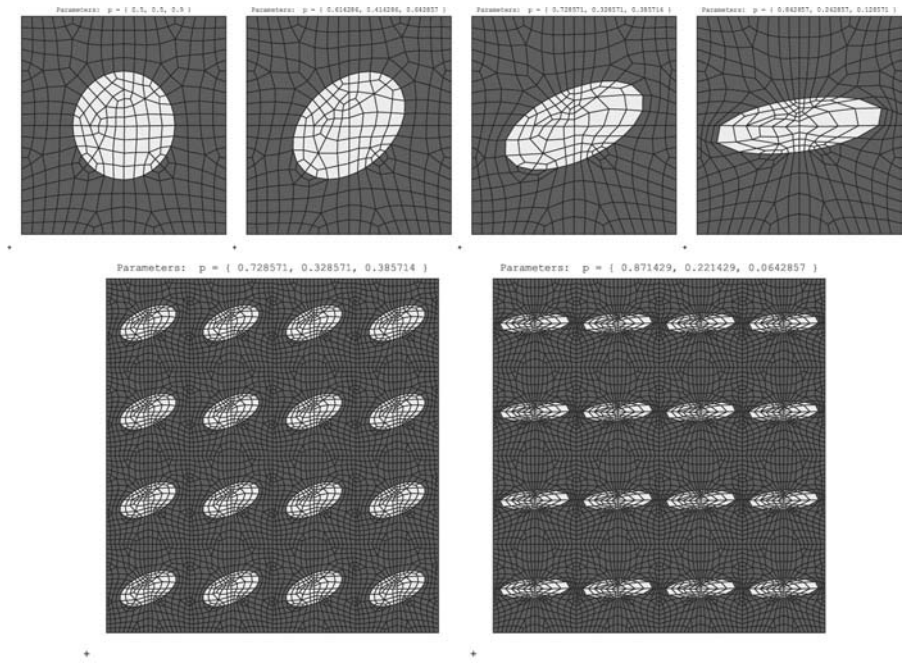

Notes: for a single periodic cell (above) and for the whole domain of the micro model (below). The first mesh above corresponds to the reference mesh with circular shape of inclusions

Figure 3.
Instances of the finite element mesh at different values of design parameters

4. Shape optimisation of microstructure

4.1 Parameterization of the shape of inclusions

In order to reduce the number of design variables, we assume periodic microstructure of the material, where the material geometry can thus be described at the micro-scale level of single periodic cell. For the model problem of two-phase material studied herein, the typical periodic cell microstructure can be defined by three-parameter representation shown in Figure 4.

By assuming the typical dimension of a period of microstructure or the size of a "cell" to be equal to d, we can start from the reference shape of the phase interface (or an inclusion contour) as a circle of radius $r_{\text{in}}(\phi) = r_0 = d/2$. At a given set of design parameters $\mathbf{p}$ the contour shape will be defined by

$$r_p(\phi, \mathbf{p}), \tag{17}$$

where (r, ϕ) are polar co-ordinates with the origin of the co-ordinate system positioned in the center of a periodic cell and r_p denotes the distance of the contour from the origin (Figure 4).

For the purpose of shape parameterization we will transform some pre-constructed reference mesh corresponding to the reference shape of inclusions according to parameter values. At any value of parameters $\mathbf{p}$ all nodes of the reference mesh will be mapped by a parameter dependent map defined over the domain of the periodic cell in

such a way that the contour of the reference inclusion shape is mapped into the contour defined by equation (17), the boundary of a periodic cell is invariant and other points are mapped $\mathbf{C}^0$ continuously with respect to co-ordinates:

$$\mathbf{x}_i(\mathbf{p}) = \tilde{\mathbf{F}}\left(\mathbf{x}_i^{(0)}, \mathbf{p}\right), \tag{18}$$

where i is a node index and $\mathbf{x}_i^{(0)}$ are the reference coordinates of the node. We will conveniently define the map in polar coordinates:

$$(r_i(\mathbf{p}), \phi_i(\mathbf{p})) = \mathbf{F}\left(r_i^{(0)}, \phi_i^{(0)}, \mathbf{p}\right). \tag{19}$$

In particular, we define $\mathbf{F}$ as

$$\mathbf{F}(r, \phi, \mathbf{p}) = \begin{cases} \left(r\dfrac{r_p(\phi, \mathbf{p})}{r_{\text{in}}(\phi)}, \phi\right); & r < r_{in}(\phi) \\ \left(r_{\text{ext}}(\phi) - (r_{\text{ext}}(\phi) - r)\dfrac{r_{\text{ext}}(\phi) - r_p(\phi, \mathbf{p})}{r_{\text{ext}}(\phi) - r_{\text{in}}(\phi)}, \phi\right); & r \geq r_{\text{in}}(\phi) \end{cases}, \tag{20}$$

where $r_{\text{in}}(\phi)$ defines the initial boundary of the inclusion,

$$r_{\text{in}}(\phi) = r_0 = d/2, \tag{21}$$

and $r_{\text{ext}}(\phi)$ defines the border of a periodic cell:

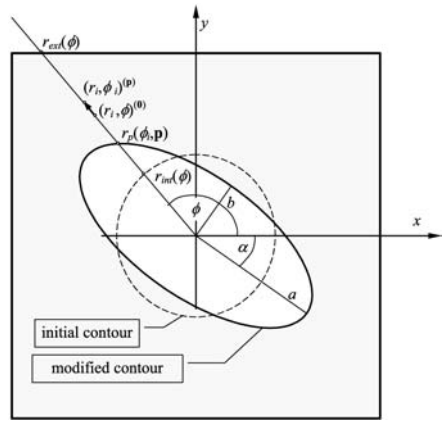

Figure 4.
A three-parameter description of the geometry of the phase interface or an inclusion in a periodic cell (note that the angle α is chosen as negative for more clear representation)

$$r_{\text{ext}}(\phi) = \begin{cases} \dfrac{d}{2\cos(\phi)}; 0 \le \phi < \dfrac{\pi}{4} \vee \dfrac{3\pi}{4} \le \phi < \dfrac{5\pi}{4} \vee \dfrac{7\pi}{4} \le \phi < 2\pi \\ \dfrac{d}{2\sin(\phi)}; \dfrac{\pi}{4} \le \phi < \dfrac{3\pi}{4} \vee \dfrac{5\pi}{4} \le \phi < \dfrac{7\pi}{4} \\ \text{periodic } (0, 2\pi); \phi < 0 \vee \phi \ge 2\pi \end{cases} \tag{22}$$

By equation (19), mesh nodes of the reference mesh are moved in radial direction. Within the inclusion domain points are contracted or stretched from the cell center towards new inclusion boundary defined by $r_p(\phi, \mathbf{p})$, while in the matrix domain points are stretched from the cell boundary towards inclusion boundary (Figure 4). $r_p(\phi, \mathbf{p})$ is defined for $[0 \le \phi \le 2\pi]$ and we require that it satisfies the following conditions:

$$\begin{aligned} & 0 < r_p(\phi, \mathbf{p}) < r_{\text{ext}}(\phi) \quad \forall \mathbf{p} \\ & r_p(0, \mathbf{p}) = r_p(2\pi, \mathbf{p}) \\ & \frac{\partial r_p}{\partial \phi}(0, \mathbf{p}) = \frac{\partial r_p}{\partial \phi}(2\pi, \mathbf{p}) \quad \forall \mathbf{p} \end{aligned} \tag{23}$$

In the examples presented in the following section we will restrict parameterization to elliptical shapes of inclusions. This is achieved by a three-parameter function

$$r_p(\phi, a, b, \alpha) = \sqrt{\frac{1}{\dfrac{\cos^2(\phi - \alpha)}{a^2} + \dfrac{\sin^2(\phi - \alpha)}{b^2}}}, \tag{24}$$

which defines an ellipse with half-axes lengths a and b and orientation specified by angle α between the main axis and the x coordinate axis (Figure 4). In order to satisfy the first condition in (22), we ought to impose the restrictions on parameter values

$$0 < |a| < d/2 \wedge 0 < |b| < d/2 \tag{25}$$

The second and third conditions in equation (23) are already satisfied by the chosen parameterization. The choice of elliptical parameterization for our study was made for several practical reasons. Possible shapes of inclusions defined in this way are simple and corresponding structures would be easy to manufacture. At the same time the variability of achievable shapes is sufficient to significantly affect the microscopic stress state and thus the overall structural response, and therefore ensure quite a significant role for optimization. Small number of design parameters allows of a better insight into the optimization process. The number of design parameters has also a critical impact on the computational cost and provides a means of filtering off high frequency oscillations in the designed shapes. This is favorable for many shape optimization applications where, in the presence of discretization and round-off errors, some means of regularization must be introduced in order to eliminate the tendency towards erroneous oscillatory solutions (Bängtsson *et al.*, 2003).

Parameterization defined by equation (24) is not unique in the sense that different sets of parameters result in the same curve. We can see, for example, that

$$\begin{aligned} &r_p(\phi, a, b, \alpha + k\pi) \equiv r_p(\phi, a, b, \alpha) \quad \forall k \in \{ZI^+ \cup ZI^-\}, \\ &r_p(\phi, b, a, \alpha + \pi/2) \equiv r_p(\phi, a, b, \alpha), \\ &r_p(\phi, -a, b, \alpha) \equiv r_p(\phi, a, b, \alpha + \pi) \end{aligned} \tag{26}$$

Unless some regularization is applied, this will inevitably lead to non-uniqueness of optimal solutions. A possible solution to this problem is to restrict the admitted set of design parameters to some set $S \subset \mathbb{R}^3$ in such a way that any pair of distinct parameter vectors within the admitted domain defines distinct shape of the inclusion, i.e.

$$\begin{aligned} &\forall \mathbf{p}_1 \in \mathbb{R}^3, \quad \forall \mathbf{p}_2 \in \mathbb{R}^3, \quad \mathbf{p}_1 \in S \wedge \mathbf{p}_2 \in S \wedge \mathbf{p}_1 \neq \mathbf{p}_1 \Rightarrow \exists \phi \in [0, 2\pi), \\ &\quad r_p(\phi, \mathbf{p}_1) \neq r_p(\phi, \mathbf{p}_2). \end{aligned} \tag{27}$$

A possible choice for S is

$$S = \{(a, b, \alpha); 0 < a < d/2 \wedge 0 \leq b < a \wedge 0 \leq \alpha < \pi\}. \tag{28}$$

In practice we do not need to bother about multiple solutions that essentially represent the same shapes. If the optimization algorithm converges to a solution that does not satisfy equation (28), we can simply transform parameter values by using identities like equation (26) in order to obtain the basic form of the solution. One can even argue that this is a better approach than to explicitly impose constraints on parameters. This can be illustrated on the hypothetical situation described below:

Let the minimized function $f(\mathbf{p})$ be of the form

$$f(\mathbf{p}) = f_s(a, b) + f_a(\alpha), \tag{29}$$

where f_s is a continuous and bounded function on $\mathbb{R}^2$ and f_α is continuous and bounded function on $\mathbb{R}$, periodic with a period 2π. Let in addition f_s attain a unique local minimum at (a^*, b^*), f_a a strict local minimum at α^* and a strict local maximum at α^+, $0 < \alpha^+ < \alpha^* < 2\pi$, and let a^* and α^+ also be global extremes of f_a. (a^*, b^*, α^*) is then a global minimum of f. Function f_a is illustrated in Figure 5. Let us restrict the set of admissible design parameters to

$$S = \{(a, b, \alpha); 0 \leq \alpha < 2\pi\}, \tag{30}$$

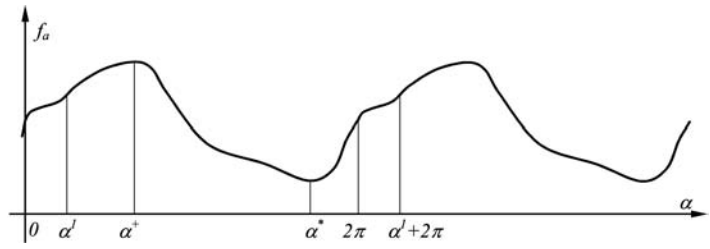

Figure 5.
A function $f_a(\alpha)$ as described in equation (29)

such that $(a^*, b^*, \alpha^*) \in S$. We can see that for any point $\alpha^1 < \alpha^+$ domain S does not contain any descent path connecting the points (a^*, b^*, α^1) and (a^*, b^*, α^*). This means that if we use a descent interior point minimization algorithm with a starting point (a^*, b^*, α^1), it will not likely converge to (a^*, b^*, α^*). In the given situation the algorithm would converge to $(a^*, b^*, 0)$. If we do not constraint the admissible range of parameters, there will exist a descent path connecting (a^*, b^*, α^1) and $(a^*, b^*, \alpha^* - 2\pi)$, and the algorithm will converge to $(a^*, b^*, \alpha^* - 2\pi)$, with the same value of the minimized function f as at (a^*, b^*, α^*).

In our case, periodicity of $f(\mathbf{p})$ in $p_3 = \alpha$ follows from the fact that points (a, b, α) and $(a, b, \alpha + 2\pi)$ of the design space represent identical designs for any a, b and α, but the assumption (29) does not generally hold. A more elaborated derivation would show that much less restrictive conditions for the minimized function and a starting guess can be defined entailing similar arguments for not restricting the parameter range in order to achieve unique parameterization.

4.2 Derivatives of the initial position of nodes with respect to shape parameters

By taking into account the transform function (20), the derivatives with respect to parameters can be written as follows:

$$\frac{\partial \mathbf{F}(r, \phi, \mathbf{p})}{\partial p_i} = \frac{\partial (\mathbf{F}_r, \mathbf{F}_\phi)}{\partial p_i} = \begin{cases} \left(\dfrac{r}{r_{\text{in}}(\phi)} \dfrac{\partial r_p(\phi, \mathbf{p})}{\partial p_i}, 0 \right); & r < r_{\text{in}}(\phi) \\ \left(\dfrac{r_{\text{ext}}(\phi) - r}{r_{\text{ext}}(\phi) - r_{\text{in}}(\phi)} \dfrac{\partial r_p(\phi, \mathbf{p})}{\partial p_i}, 0 \right); & r \geq r_{\text{in}}(\phi) \end{cases} \tag{31}$$

In equation (31), (r, ϕ) refer to polar coordinates of nodes in the referential mesh. If $r_p(\phi, \mathbf{p})$ is defined by (23), then its derivatives with respect to parameters (the half-axes of the ellipse and the angle between the first half-axis and the x direction) are as follows:

$$\begin{aligned} \frac{\partial r_p(\phi, \mathbf{p})}{\partial p_1} &= \frac{\partial r_p(\phi, a, b, \alpha)}{\partial a} \\ &= \frac{\cos(\phi - \alpha)^2}{a^3} \sqrt{\frac{1}{\dfrac{\cos(\phi - \alpha)^2}{a^2} + \dfrac{\sin(\phi - \alpha)^2}{b^2}}}^3 \end{aligned} \tag{32}$$

$$\begin{aligned} \frac{\partial r_p(\phi, \mathbf{p})}{\partial p_2} &= \frac{\partial r_p(\phi, a, b, \alpha)}{\partial b} \\ &= \frac{\sin(\phi - \alpha)^2}{b^3} \sqrt{\frac{1}{\dfrac{\cos(\phi - \alpha)^2}{a^2} + \dfrac{\sin(\phi - \alpha)^2}{b^2}}}^3 \end{aligned} \tag{33}$$

$$\frac{\partial r_p(\phi,\mathbf{p})}{\partial p_1} = \frac{\partial r_p(\phi,a,b,\alpha)}{\partial a} = \left(\frac{\cos(\alpha-\phi)\sin(\alpha-\phi)}{a^2} - \frac{\cos(\alpha-\phi)\sin(\alpha-\phi)}{b^2}\right) \times \sqrt{\frac{1}{\frac{\cos(\phi-\alpha)^2}{a^2}+\frac{\sin(\phi-\alpha)^2}{b^2}}}^{3} \tag{34}$$

At each design iteration we reconstruct the mesh for subsequent mechanics analysis by applying the transform in equation (20) to all nodes of the given reference mesh, which implies that all the nodal co-ordinates in the mesh are readily available. Another possible approach is to just use the parametric definition of the boundary between the inclusion and the matrix and generate the mesh upon this boundary. In order to calculate the derivatives of the nodal positions with respect to the shape parameters, we must first transform the positions of nodes produced by the mesh generation procedure to the referential co-ordinates in which the transform $\mathbf{F}$ is defined[1]. For this we must construct the inverse map $\mathbf{F}^{-1}$ defined in such a way that $\mathbf{F}^{-1}(\mathbf{F}(r,\phi,\mathbf{p}),\mathbf{p}) = (r,\phi)$. For the shape defined by transform in equation (20) we have

$$\mathbf{F}^{-1}(\tilde{r},\tilde{\phi},\mathbf{p}) = \begin{cases} \left(\tilde{r}\dfrac{r_{\text{in}}(\phi)}{r_p(\phi,\mathbf{p})},\phi\right); & \tilde{r} < r_p(\phi,\mathbf{p}) \\ \left(\dfrac{\tilde{r}(r_{\text{ext}}(\phi)-r_{\text{in}}(\phi))+r_{\text{ext}}(\phi)r_{\text{in}}(\phi) - r_{\text{ext}}(\phi)r_p(\phi,\mathbf{p})}{r_{\text{ext}}(\phi)-r_p(\phi,\mathbf{p})},\phi\right); & \tilde{r} \geq r_p(\phi,\mathbf{p}) \end{cases}, \tag{35}$$

4.2.1 Transformation to Cartesian coordinates. Since the calculation will be performed in Cartesian coordinates, we need to transform $\mathbf{F}$ and its derivatives. The polar and Cartesian coordinates are related by

$$x = r\cos(\phi),\ \ y = r\sin(\phi) \quad r = \sqrt{x^2+y^2}, \phi = \begin{cases} \text{arctg}\, y/x;\ \ x > 0 \\ \pi + \text{arctg}\, y/x;\ \ x < 0 \\ \dfrac{\pi}{2};\ \ x = 0 \wedge y > 0 \\ \dfrac{3\pi}{2};\ \ x = 0 \wedge y < 0 \\ 0;\ \ x = y = 0 \end{cases} \tag{36}$$

4.3 Imposing geometric constraints by intermediate transforms

By application of transforms like equation (20) a bad input mesh for finite element calculation can be obtained. Geometrically infeasible situation occurs when parts of

the inclusion boundary exceeds the cell boundary. Unfavorable mesh can be produced even if the geometric layout is physically permissible, because the transform can distort individual elements in such a way that angles between adjacent element edges are larger than π radians (Figure 6).

Two corrective mechanisms were used in order to prevent excessive mesh distortion, both of which utilize additional intermediate maps. The first correction is performed by application of an intermediate map directly to shape parameters in order to keep them in a given range where mesh distortion is not so severe. The second correction is performed by additionally transforming the co-ordinates of the inclusion boundary in such a way that it cannot exceed the boundary of the cell. In the case where the first correction would not prevent the inclusion boundary of extending out of the cell, the second correction would produce non-elliptical shapes, thus modifying the intended set of attainable shapes. The role of the second correction is twofold: first it prevents the breakdown of the optimization algorithm when infeasible guesses are generated, and second it can produce instructive results worth of further analysis when the optimal point lies in the extreme portions of parameter space where the correction becomes effective.

The corrections are performed by transforming the parameters or co-ordinates by monotonous functions with a limited range. For example, lower and upper bound on an individual parameter are enforced by setting

$$p_i(\tilde{p}_i) = f_1(\tilde{p}_1, l_{\min}, l_{\max}, d), \tag{37}$$

where $\tilde{p}_i$ is an optimization parameter, p_i is the transformed value of this parameter actually used in the shape transform formulae, f_l is the family of functions used for enforcing the bounds on parameter range, and constant parameters of the family $l_{\min}$, $l_{\max}$ and d specify the lower, the upper bound and the transition interval, respectively. $f_1(\tilde{p}_i, \ldots)$ must be monotonously increasing function of $\tilde{p}_i$, with

$$f_1(p_i, l_{\min}, l_{\max}, d) \in [l_{\min}, l_{\max}] \tag{38}$$

Since the optimization algorithm operates with parameters $\tilde{\mathbf{p}}$ rather than $\mathbf{p}$, we must apply the chain rule in order to calculate the derivatives of the initial co-ordinates of mesh nodes with respect to the parameters. Instead of $\mathbf{F}(r, \phi, \mathbf{p})$, the actual co-ordinate transform is

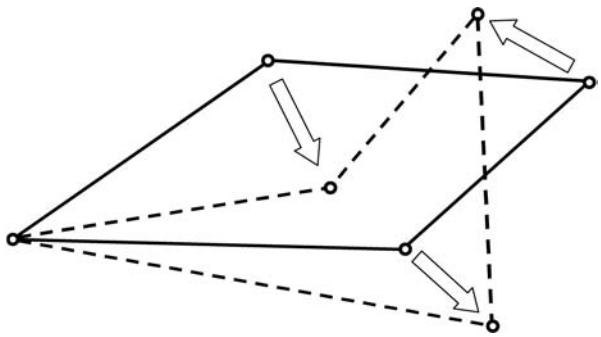

Figure 6.
Undesired distortion of a mesh element by the shape transform

$$\tilde{\mathbf{F}}(r, \phi, \tilde{\mathbf{p}}) = \mathbf{F}(r, \phi, \mathbf{p}(\tilde{\mathbf{p}})). \tag{39}$$

Considering equations (31) and (37), we have:

$$\frac{\mathrm{d}\tilde{\mathbf{F}}(r, \phi, \mathbf{p}(\tilde{\mathbf{p}}))}{\mathrm{d}\tilde{p}_i} = \frac{\partial \tilde{\mathbf{F}}(r, \phi, \mathbf{p})}{\partial p_i} \frac{\mathrm{d}f_1(\tilde{p}_i, l_{i\min}, l_{i\max}, \mathrm{d}_i)}{\mathrm{d}\tilde{p}_i}. \tag{40}$$

Geometrically feasible bounds on the co-ordinates of the transformed mesh were achieved by enforcing suitable bounds on the inclusion boundary $r_p(\phi, \mathbf{p})$. As in equation (37), this was accomplished by application of an additional function with a limited range to the inclusion boundary determined by equation (24). We will write

$$\bar{r}_p(\phi, \mathbf{p}(\tilde{\mathbf{p}})) = f_1(r_p(\phi, \mathbf{p}(\tilde{\mathbf{p}})), r_{p\min}(\phi), r_{p\max}(\phi), \mathrm{d}(\phi)). \tag{41}$$

Accordingly, we must replace $r_p(\phi, \mathbf{p})$ with $\tilde{r}_p(\phi, \tilde{\mathbf{p}})$ in the formulae (20), (31) and (35), and $\partial r_p(\phi, \mathbf{p})/\partial p_i$ with $\partial \bar{r}_p(\phi, \tilde{\mathbf{p}})/\partial \tilde{p}_i$. The last derivative is obtained as

$$\begin{aligned} \frac{\partial \bar{r}_p(\phi, \mathbf{p}(\tilde{\mathbf{p}}))}{\partial \tilde{\mathbf{p}}_i} &= \frac{\partial \bar{r}_p(\phi, \mathbf{p}(\tilde{\mathbf{p}}))}{\partial r_p} \frac{\partial r_p}{\partial p_i} \frac{\mathrm{d}p_i}{\partial \tilde{\mathbf{p}}_i} \\ &= \frac{\partial f_1(r_p(\phi, \mathbf{p}), r_{p\min}(\phi), r_{p\max}(\phi), d_p(\phi))}{\partial r_p}\bigg|_{\phi, \tilde{p}} \frac{\partial r_p}{\partial p_i}\bigg|_{\phi, \tilde{p}} \frac{\mathrm{d}f_1(\tilde{p}_i, l_{i\min}, l_{i\max}, d_i)}{\mathrm{d}\tilde{p}_i}. \end{aligned} \tag{42}$$

The same family of functions was used for imposing bounds on $\bar{r}_p$ as for imposing limits on parameter range, and

$$\mathbf{p}(\tilde{\mathbf{p}}) = (p_1(\tilde{p}_1), p_2(\tilde{p}_2), \ldots),$$

i.e. each transformed p_i depends only on one corresponding parameter $\tilde{p}_i$. We allow the parameters of the family to be dependent on ϕ. In this way, we can for example set the upper bound for inclusion boundary to be a square slightly smaller than the periodic cell, i.e. defined by a formula similar to equation (22), except with a smaller d.

4.4 Transforms used for limiting parameter range and inclusion boundary

As mentioned before, functions f_i must be monotonously increasing functions of the first argument for any parameter of the family. It must be continuously differential with respect to the first argument. Furthermore, we design functions in such a way that

$$\min + d < x < \max - d \Rightarrow f_1(x, \min, \max, d) = x. \tag{43}$$

The functions are conveniently defined by gluing together monotonous segments that are adequately bound and satisfy the continuity conditions at the endpoints. The following form with continuous second derivatives has been chosen in the particular case:

$$f_1(x,\min,\max,d)=\begin{cases}\min;\ \ x\le\min-d\\ \min+fc1(x-(\min-d),d);\ \ \min-d<x\le\min\\ \min+fc2(x-(\min+d),d);\ \ \min<x<\min+d\\ x;\min+d\le x\le\max-d\\ \max-fc2((\max-d)-x,d);\ \ \max-d<x<\max\\ \max-fc1((\max+d)-x,d);\ \ \max\le x<\max+d\\ \max;\ \ \max+d\le x\end{cases} \tag{44}$$

The corresponding derivative and inverse formulas are

$$\frac{\mathrm{d}f_1(x,\min,\max,d)}{\mathrm{d}x}=\begin{cases}0;\quad x\le\min-d\\ \mathrm{der}fc1(x-(\min-d),d);\ \ \min-d<x\le\min\\ \mathrm{der}fc2(x-(\min+d),d);\ \ \min<x<\min+d\\ 1;\quad \min+d\le x\le\max-d\\ \mathrm{der}fc2((\max-d)-x,d);\ \ \max-d<x<\max\\ \mathrm{der}fc1((\max+d)-x,d);\ \ \max\le x<\max+d\\ 0;\ \ \max+d\le x\end{cases} \tag{45}$$

and

$$f_1^{-1}(y,\min,\max,d)=\begin{cases}\min-d;y\le\min\\ \min-d+\mathrm{inv}fc1(y-\min,d);\ \ \min<y\le\min+d/6\\ \min+d+\mathrm{inv}fc2(y-\min,d);\ \ \min+d/6<y<\min+d\\ y;\ \ \min+d\le y\le\max-d\\ \max-d-\mathrm{inv}fc2(\max-y,d);\ \ \max-d<y<\max-d/6\\ \max+d-\mathrm{inv}fc1(\max-y,d);\ \ \max-d/6\le y<\max\\ \max+d;\ \ \max\le y\end{cases}, \tag{46}$$

where the family of inverse functions f_l^{-1} is defined by the formula

$$f_1^{-1}(f(x,\min,\max,d),\min,\max,d)=x. \tag{47}$$

The functions f_1, its first and second derivatives and its inverse are shown in Figure 7. Auxiliary functions used in the definition of f_l are defined as follows:

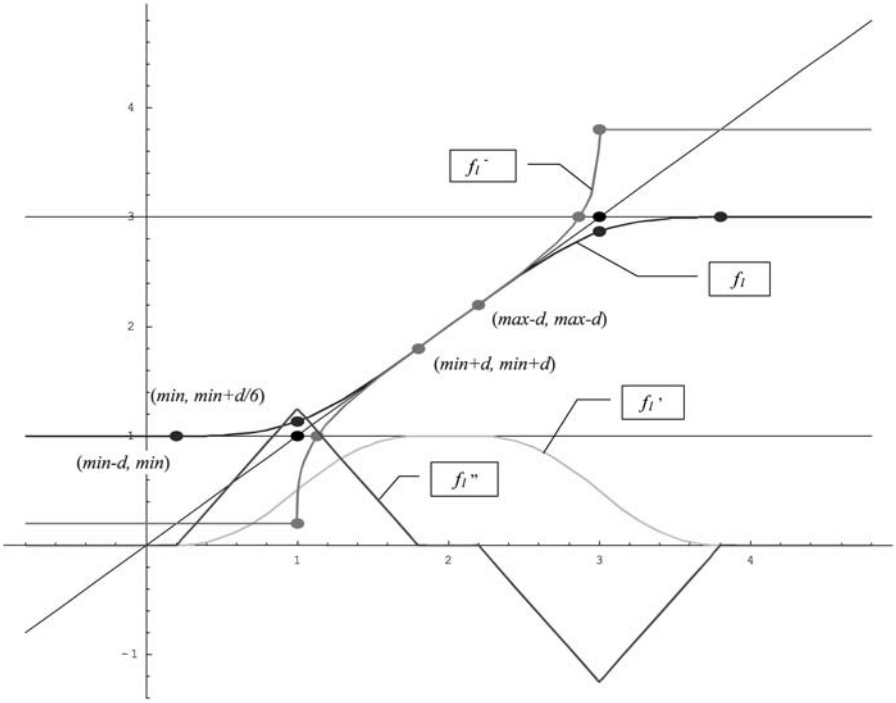

Figure 7.
The function used for limiting parameter range with its first and second derivative and inverse

$$
\begin{aligned}
&fc1(x,d) = \frac{x^3}{6d^2},\\
&fc2(x,d) = d + x - \frac{x^3}{6d^2}\\
&\mathrm{der}fc1(x,d) = \frac{\mathrm{d}fc1(x,d)}{\mathrm{d}x} = \frac{x^2}{2d^2}\\
&\mathrm{der}fc2(x,d) = \frac{\mathrm{d}fc2(x,d)}{\mathrm{d}x} = 1 - \frac{x^2}{2d^2}\\
&\mathrm{inv}fc1(y,d) = \sqrt[3]{6d^2y}\\
&\mathrm{inv}fc21(y,d) = x;\ \ fc2(x,d) = y \wedge x \in [-d,0]
\end{aligned}
\tag{48}
$$

The value of inv*fc*21 is obtained by application of the analytical formula for zeros of a third order polynomial and choosing the real solution that lies in the appropriate interval $[-d,0]$. There is always exactly one such value for the interval $y \in [d/6,d]$ where inv*fc*2 is evaluated, since *fc*2 is strictly monotonous on $[-d,0]$ with derivative lying in $[1/2,1]$.

5. Numerical examples

Several numerical examples are chosen and solved in order to demonstrate the applicability of the proposed design approach. While application to design of a material with far more complex microstructure can be foreseen for many practical situations, the main goal of the presented numerical experiments was to validate the solution scheme for the chosen model material with two-phase microstructure. In particular, feasibility of combining multi-scale numerical models, featuring elasto-plastic and damage material phases at the smaller scales, with efficient gradient-based techniques for constrained optimization was investigated. We also wanted to draw some attention to problems previously experienced in the area of material forming (Grešovnik, 2000; Grešovnik and Rodič, 2003), such as the presence of substantial noise in the numerical response that can badly affect the performance of classical optimization algorithms.

A structural element under a given loading (prescribed displacements) was considered, as depicted in Figure 8. The element is composed of a matrix containing periodically distributed inclusions of a different material. The material properties of the matrix are described by the von Mises elasto-plastic model, using the following yield function, Φ^p,

$$\Phi^p(\sigma, q^p) = \|\mathrm{Dev}(\sigma)\| - \sqrt{\frac{2}{3}}(\sigma_y + q^p), \tag{49}$$

where $\mathrm{Dev}(\sigma) = \sigma - 1/3\,\mathrm{Tr}(\sigma)I$ is the deviatoric part of the stress σ, $\mathrm{Tr}(\sigma)$ is its trace and I the 3×3 identity matrix. In equation (49) σ_y represents the initial yield stress and q^p the plastic hardening function, defined as

$$q^p(\xi^p) = (\sigma^p \infty - \sigma_y)(1 - e^{-b^p \xi^p}), \tag{50}$$

where ξ^p is the hardening variable, σ^p_∞ the plastic saturation stress and b^p the plastic saturation exponent. In our analyses the matrix material parameters take the following values: $\sigma_y = 1.0\,10^8$, $\sigma^p_\infty = 5.0\,10^8$, $b^p = 1,000$.

On the other hand, the behavior of inclusions is described by the damage model introduced in Ibrahimbegovic *et al.* (2003) and very similar to the classical plasticity model described above. It is based on the fracture criterion function, Φ^d,

$$\Phi^d(\sigma, q^d) = \mathrm{Tr}(\sigma) - (\sigma_f + q^d), \tag{51}$$

where σ_f represents the initial fracture stress and q^d the damage hardening function, defined as

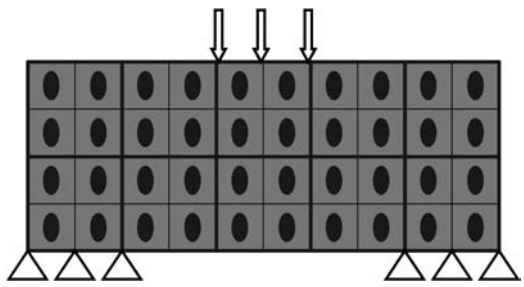

Figure 8.
Studied heterogeneous structure with periodic microstructure

$$q^d(\xi^d) = (\sigma_\infty^d - \sigma_f)(1 - e^{-b^d \xi^d}), \tag{52}$$

with ξ^d being the damage hardening variable and σ_∞^d, b^d are damage saturation stress and damage saturation exponent, respectively. In our analyses the inclusion material parameters take the following values: $\sigma_f = 0.33 \times 10^8$, $\sigma_\infty^d = 0.66 \times 10^8$, $b^d = 10$. The corresponding linear and isotropic elastic properties of each phase are $K^p = 1.0 \times 10^{10}$ (matrix bulk modulus), $G^p = 1.0 \times 10^{10}$ (matrix shear coefficient), $K^d = 1.2 \times 10^{10}$ (inclusion bulk modulus) and $G^d = 1.5 \times 10^{10}$ (inclusion shear coefficient).

We optimized the shape of inclusions with respect to different criteria regarding the overall response of the element. Elliptical shapes of inclusions were considered using the parameterization described in Section 4. The numerical model was described in Section 2 and the solution scheme in Sections 3 and 4.

Preliminary testing of the method was performed on problems with trivial solutions that can be guessed in advance. Namely, when the objective function pertains to maximizing the plastic dissipation, the optimal design which follows is the one where the inclusion size shrinks to zero and the matrix material occupies the whole domain. On the contrary, when we look for the design at which the work of external forces is maximal, the optimal solution implies that the inclusion material would occupy the whole space.

Figure 9 shows the solutions obtained for both of these cases represented by the finite element mesh of the periodic cell. The applied parameterization is not capable of representing these extreme situations and the algorithm therefore converges to the representative designs with minimum and maximum inclusion volumes, respectively. The half-axes of the inclusion were not formally constrained in this case. Instead, the *a priori* constraints were imposed on the inclusion boundary by application of additional transforms on the boundary radius $r_p(\phi, \mathbf{p})$ as described in the previous section (see equation (41)). More precisely, $r_{p\min}(\phi)$ defining the boundary of the smallest possible inclusion was chosen as a circle with a very small radius and $r_{p\max}(\phi)$ was chosen to be a square with the side a bit smaller than width the periodic cell. The latter was chosen intentionally in order to make the effect of the transform visually more apparent.

The problem of excessive mesh distortion for each of these two designs is clearly visible in Figure 9(b). In spite of such drastic situation regarding the finite element

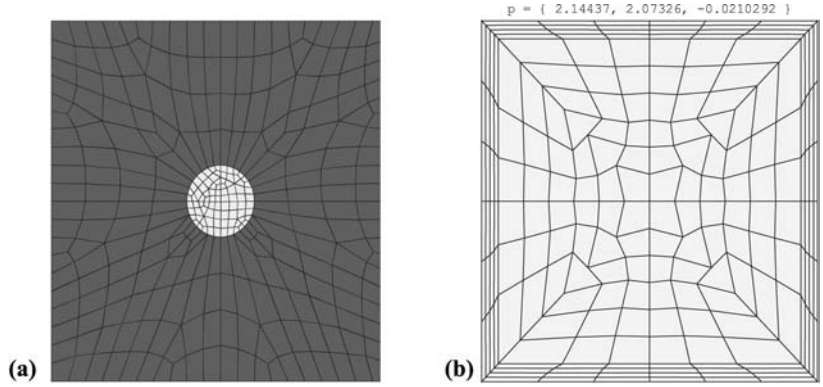

Figure 9.
Finite element mesh of the periodic cell at the solutions: (a) when maximizing total plastic dissipation; and (b) when maximizing work of external forces

mesh distortion, no problems were experienced with convergence of the optimization procedure to the expected result. However, one should take into account that the results obtained by the finite element analysis are rather sensitive to mesh distortion and therefore a control on the mesh grading and mesh regularity should be incorporated accordingly when applying the approach described herein. More precisely, with the proposed solution scheme and flexible software architecture, it is easy to calculate and manipulate numerical indicators of mesh regularity within the optimization procedure. Such indicators can either be used just to provide information on when the results should no longer be too much trusted, or to actively control the optimization procedure, e.g. by using the penalty terms, in order to always force the design problem solution and subsequent mesh distortion within the range which can be considered as acceptable with respect to the mechanics simulation results remaining of sufficient accuracy. In the presented examples, we used the Pian-Sumihara elements (Pian and Sumihara, 1984) in the microscopic finite element model, which are known to be rather insensitive to shape irregularity.

Different approaches can be imagined to deal with situations where excessive mesh distortion would prevent the determination of optimal solution providing the equivalent accuracy of result that is otherwise possible with respect to the accuracy of the numerical simulation of mechanics problem. Although a more detailed exploration is beyond the scope of the present work, we would like to mention two possibilities that we deem convenient for practical applications. The first possibility is to apply automatic mesh generation in order to generate the mesh for the micro level, and thus apply the shape transform described in the previous section only to the geometrical definition of the inclusion boundary. Positions of the internal mesh nodes would be in this case produced without explicit application of the shape transforms. However, we would still need to consider the explicit definition of the transforms to provide the consistent sensitivity fields over the interior of the matrix or inclusion material in the case of sensitivity analysis. In this case, the positions of generated mesh nodes should be mapped to the reference domain by the inverse transform in order to calculate derivative terms. The only additional implementation difficulty that we are able to foresee is in interfacing and manipulation of the geometry definition of the boundary and related automatic mesh generation. Sufficient tools to implement such an approach are already available in any commercial simulation environment. One must, however, anticipate that such an approach would reduce the efficiency of the optimization procedure because of the addition of non-smoothness to the numerically calculated relation between the design parameters and the objective and constraint functions. Transforming the same reference mesh over several analyses, and re-meshing only (a very few times) when the mesh becomes too distorted, should be able to alleviate these problems. According to our experience, such approach is well suited already at least for the chosen example problems. In all demonstrated cases, a single re-meshing is sufficient mesh quality, and furthermore even manual intervention would be quite adequate.

Another possibility to deal with the problem of mesh distortion is to use a fixed regular mesh over the complete domain of the periodic cell. In this case, material composition and representation of the interface between the matrix and inclusion material would be dealt with at the level of an individual element rather than on the element interface level. This kind of structured mesh representation of

the microstructure, as proposed in Ibrahimbegovic and Markovic (2003), would provide an important advantage of mesh regularity and prevent any possibility of mesh distortion and resulting ill-conditioning problem. However, the number of design variables would increase considerably with respect to the exact finite element representation employed herein, since any micro-scale element would become a potential candidate for harboring an interface between two phases and the corresponding design variables describing it. In the present case with a regular, elliptic shape of phase interface, which can be described with only three design variables, the structured mesh approach is very unlikely to be more efficient. However, when considering the best shape representation of the phase interface in a more general case with a multi-phase composite material, the latter approach should not be discarded *a priori*.

The two above mentioned example problems of interface shape optimization were first solved by the Nelder-Mead simplex method. Rather than a single point, this method maintains a set of $n+1$ points where the objective function is evaluated through iterations, where n is the number of parameters. An instance of the solution path in the parameter space is shown in Figures 10 and 11, for the example with solution shown in Figure 9(b). Convergence of the value of the objective function and distance from the optimum is shown in Figure 12.

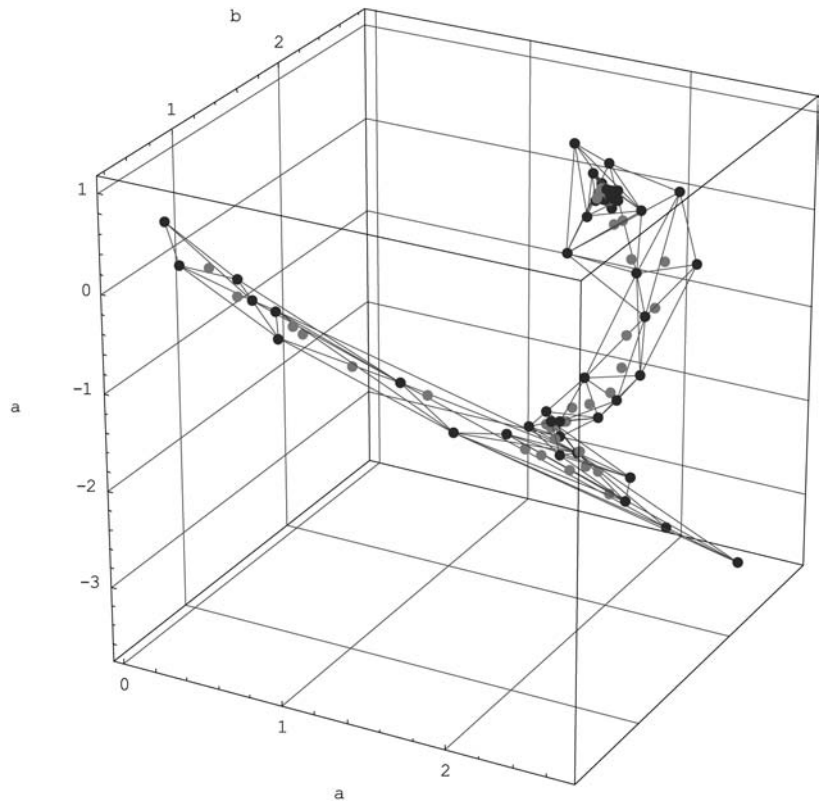

Figure 10.
Solution path of the Nelder-Mead simplex method in the space of shape parameters. Edges and apices of the subsequent simplexes are shown, together with their centers (red points)

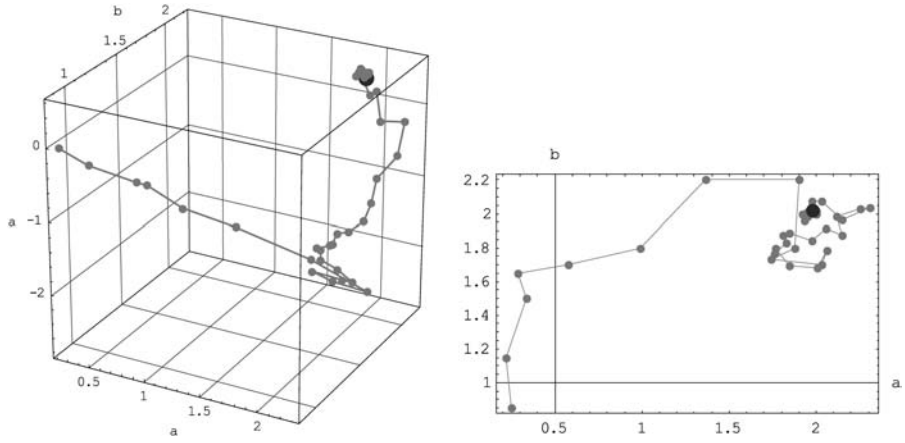

Figure 11.
Solution path defined by centers of simplexes shown in the previous figure. Projection to the sub-space of ellipse half-axes is shown on the right-hand side

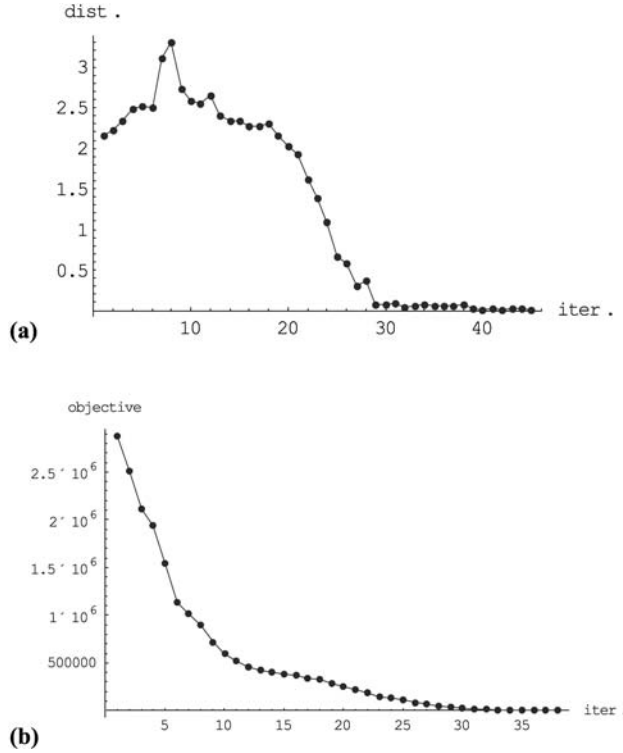

Figure 12.
Convergence of the simplex method: (a) distance from the optimum; and (b) value of the objective function

These calculations typically converged with the precision of 10^{-3} taking in between 50 and 100 iterations (which corresponds to about 100-200 evaluations of the objective function). Different starting points were set in order to check that the algorithm converges to the same point. For the two example problems, the solution was not unique in terms of the optimal angle of the "elliptical" inclusion, since all angles resulted in the same symmetric shape due to the imposed parameter transform. In terms of the finite element mesh, various solutions agreed almost exactly. Non-uniqueness in terms of calculated optimal parameters is very unlikely to be observed in complex cases.

Typical computation times for a single analysis run, carried out in parallel on eight 2.4 GHz Pentium 4 Linux workstations, ranged between 5 and 8 min. Bookkeeping time of the optimization algorithm is negligible for the proposed solution scheme; therefore, the main opportunity for improving the efficiency was seen in reduction of the number of required analyses by application of a more efficient optimization algorithm. The sequential quadratic programming (SQP, Fletcher, 1996; Lawrence and Tits, 1996) was the method of choice for its known performance in solving non-linear constrained problems. Our main concerns related to the application of this method were related to potentially noisy calculated response, especially because we calculated the derivatives of the objective and constraint functions numerically by the forward difference method. We therefore investigated behavior of the calculated response in this respect by preliminary parametric studies.

Some results of these studies are shown in Figures 13-18. We examined angular dependency of the calculated response with fixed size of half-axes of the ellipse (Figures 13 and 14). These tests indicated that the total response of the loaded structure significantly depends on the orientation of the inclusions, rather than mainly on the inclusion volume.

Further computations are made to get some indication on the level of noise in computed response, which is obtained by tabulating the response in the parameter space. The goal is to find out at what range of parameter change the contribution of

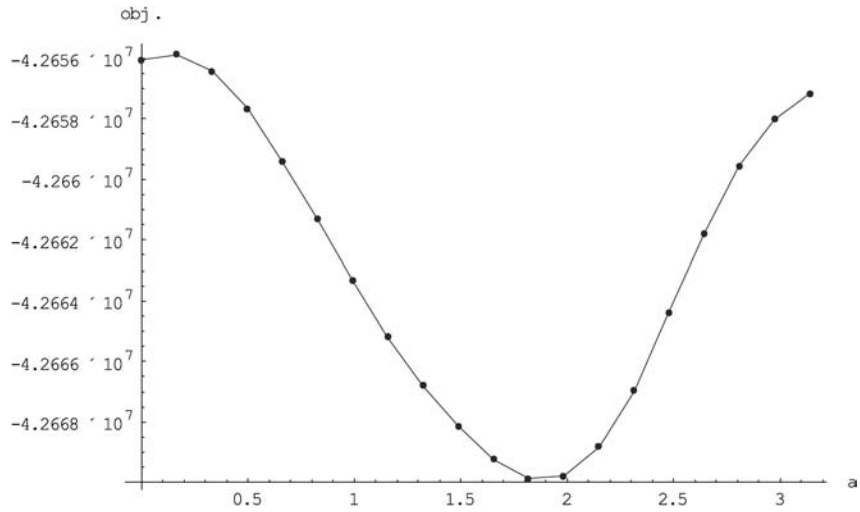

Figure 13.
Dependence of minus total plastic dissipation on the inclination angle of the inclusion. Half-axes were fixed at $a = 0.3$ and $b = 0.6$

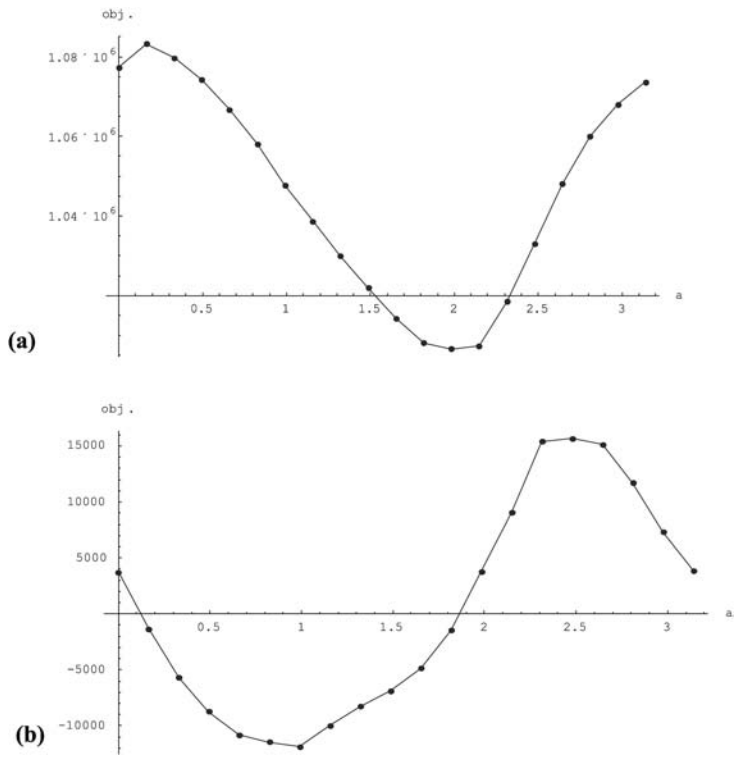

Figure 14.
Dependence on the inclination angle of the inclusion of the derivative of minus plastic dissipation with respect to: (a) the larger half-axis; and (b) the inclination angle

numerical noise is qualified as being considerable with respect to the local trend in the response. This information was crucial for the choice of step for numerical differentiation for objective function derivative computation. Since little can be concluded in advance, the chosen approach is simply to tabulate the response along individual parameters over different interval lengths, with sufficient number of points along each interval to be able to visualize the effect of noise and distinguish it from the general trend.

Because of well-scaled design parameters, tabulating along directions such that all parameters change equally should give as useful first indications as tabulating along individual parameters. For better efficiency, we also replaced several uniform samplings on increasingly shorter lines by a sampling with intervals of geometrically increasing length. For the first indication of the effect of numerical noise, we performed the tabulation of calculated response starting at parameters $\mathbf{p}_1 = [0.3, 0.6, 0.1]^{\mathrm{T}}$ and ending at $\mathbf{p}_2 = [0.29, 0.61, 0.11]^{\mathrm{T}}$. We sampled in 30 points, by a rather conservative factor of interval length growth of 1.2. This implies the length of the first sampling interval being about 0.1 percent and the length of the last sampling interval being about 17 percent of the whole interval. Sampling by factors of interval growth of two or more is usually adequate for this task and much more efficient, but a bit less comfortable for visualization. Figure 15 shows the variation of minus plastic dissipation along a given direction between the two points. No effect of random noise

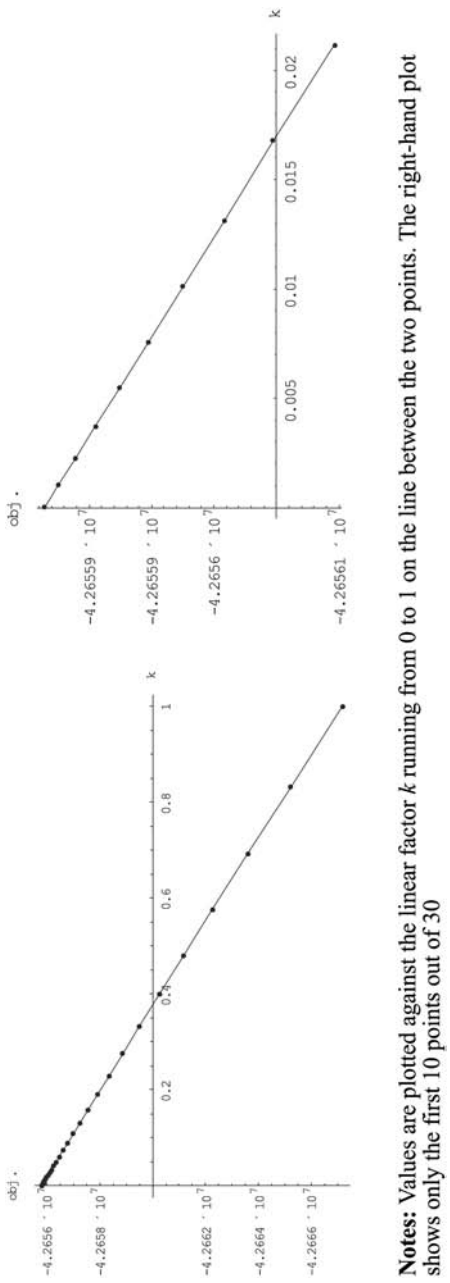

Notes: Values are plotted against the linear factor *k* running from 0 to 1 on the line between the two points. The right-hand plot shows only the first 10 points out of 30

Figure 15.
Variation of minus plastic dissipation along the straight line between the points $p_1=[0.3,0.6,0.1]^T$ and $p_2=[0.29,0.61,0.11]^T$ in the space of shape parameters *a, b and a*

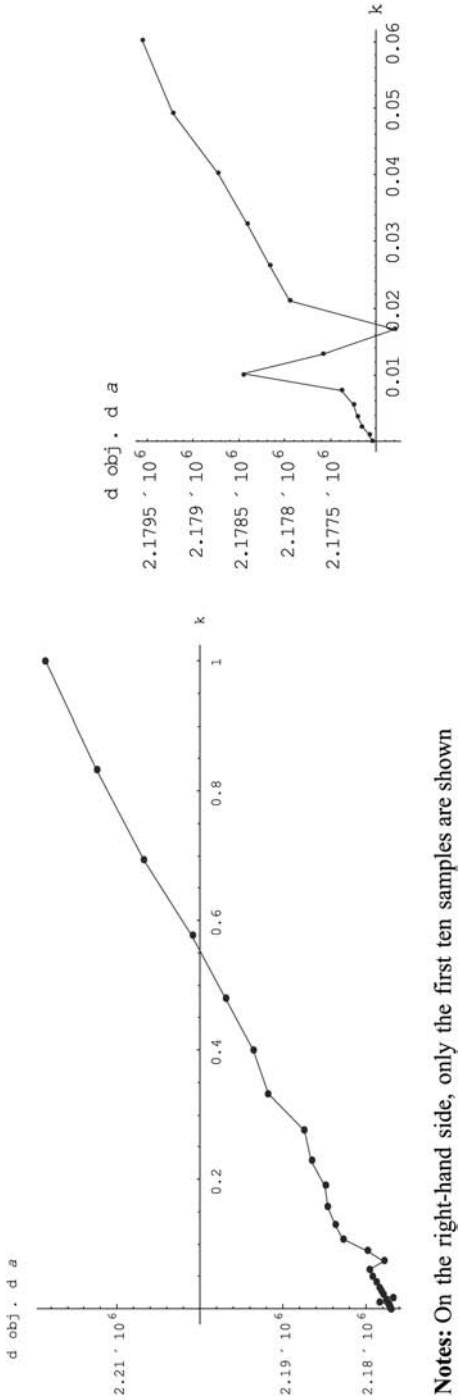

Notes: On the right-hand side, only the first ten samples are shown

Figure 16.
Numerical derivative of minus plastic dissipation with respect to the first half-axis sampled in the same points as the results shown in earlier

patterns can be perceived on the plots, indicating that it should be appropriate to use numerically calculated derivatives in the optimization procedure.

We have fixed the length of the interval for numeric differentiation at 0.001 for all three parameters and verified the suitability of this choice by tabulating the numerical derivatives obtained by forward differentiation. Results are shown in Figures 16 and 17 for derivatives with respect to the first axis and the inclination angle, respectively. Sampling was performed in the same way as described above for the results in Figure 15. Results for derivatives with respect to the second half-axis are similar as those for the first half-axis shown in Figure 16. We can see that the amplitude of what appears to be the contribution of non-smooth response is less than 1/10 of the difference in the derivative with respect to the first axis between the points $\mathbf{p}_1$ and $\mathbf{p}_2$. This is encouraging, especially if we take into account that the variation of the first parameter is opposite to the variation of the second one, effectively compensating the terms dependent just on the size of the inclusion.

Differentiation with respect to the inclination angle is more critical, obviously because the sensitivity with respect to this parameter is about two orders of magnitudes smaller (see Figure 17) than the sensitivity with respect with the first two parameters. We have therefore chosen to increase the step length for numerical differentiation with respect to this parameter to 0.01.

We applied the so-called feasible sequential quadratic programming, a variant of the SQP algorithm developed by Tits *et al.* (Panier and Tits, 1993; Lawrence and Tits, 1996;

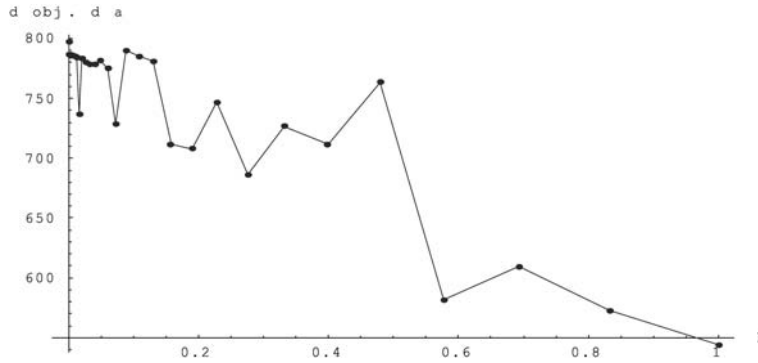

Figure 17.
Numerical derivative of minus plastic dissipation with respect to the inclination angle

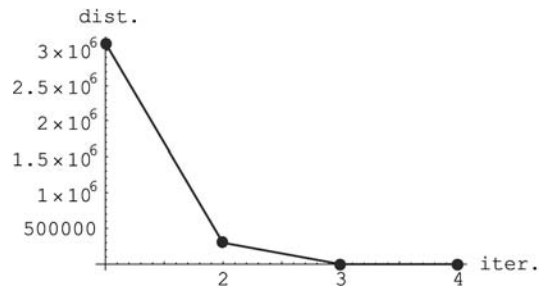

Figure 18.
Convergence of the objective function for the problem whose solution is shown in Figure 9(b)

Bonnans *et al.*, 1992; Lawrence *et al.*, 1995), with forward difference numerical differentiation to solve a series of problems with different objectives and constraints. For unconstraint problems the method is reduced to the Broyden-Fletcher-Goldfarb-Shanno (BFGS) non-linear minimization algorithm with line search (Fletcher, 1996; Dennis and Schnabel, 1996). It was applied to the same problem whose solution by the simplex method was described above, i.e. maximization of the work of external forces (Figure 9(b)). The solution of this problem was typically obtained in three to four iterations (Figure 12), which took less than 50 numerical analysis runs in total. Four analyses were run for each point of the parameter space to calculate the objective function and its gradient.

In the considered example with simple geometry and loading, various measures of overall performance such as work of external forces or plastic dissipation exhibit monotonous dependency on the volumetric ratio of the two phases and therefore size of inclusions, at any fixed shape and orientation of inclusions. Designs of microstructure obtained by minimization or maximization of such measures will correspond to designs with maximal or minimal volume of one phase, such as those shown in figure. We regard here only those geometric layouts that are elements of the design space defined by a chosen parameterization, and the solutions with minimal or maximal volume of a given space do not necessarily coincide with layouts where one phase vanishes. It is interesting to consider problems where we look for minimum of a given criterion, while a set of feasible designs is constrained with another criteria. We deal with such examples below. The choice of criteria was not motivated by any particular application, and the primary purpose of the examples is to examine the proposed solution scheme.

We first look for the design that results in maximal plastic dissipation, with a prescribed upper limit on the accumulated damage. For chosen materials, both damage and plastic dissipation grow with the size of inclusion and are relatively more sensitive to size than orientation. We can expect that the constraint will be active in the optimum while exact orientation and half-axes will be adjusted according to local dependency of both damage and plastic dissipation, thus hard to be guessed or determined by manual parametric studies. *A priori* bounds on the half-axes were imposed implicitly by transformation of parameters (equations (37), (38), (44) and (48)). Lower bound of 0.15 and upper limit of 0.9 were imposed for both half-axes. We also wanted to avoid excessively elongated, oblong inclusion shapes and therefore, we applied additional parameter transform of this type that constrained achievable ratios between half-axes to at most 2.5. It turned that both explicit constraint on the allowed amount of damage and the imposed bound on half-axes ratio determined the optimal shape, which is shown in Figure 19. Optimal parameters were $[0.254, 0.95, 3.205]^{\mathrm{T}}$, which corresponds to geometric parameters $a \approx 0.634$, $b \approx 0.254$ and $\alpha \approx 1.635$. These values were, in addition to the bound imposing transform, obtained by swapping half-axes and rotating by $\pi/2$ clockwise, in order to provide a unique notation.

The FSQP algorithm converged to this solution in up to ten iterations from different starting points, with 15-20 evaluations of the objective and constraint functions and their gradients. Since gradients were calculated numerically, each evaluation took five complete numerical analyses of the structure and the actual computational cost was up to 80 analyses. In this case, the optimum obtained in subsequent experiments was

unique within the prescribed tolerance. Figure 20 shows an instance of the convergence path of the method, while variation of the distance from the optimum and values of the objective and constraint function is shown in Figure 21.

In Figures 22 and 23 the results for the same solution procedure are represented, but this time all evaluations are shown, including those performed in the line searches.

Two other problems were considered: maximization of plastic dissipation with constraint on maximum volume (Figure 24(a)) and minimization of plastic dissipation with constraint on the minimum work of external forces (Figure 24(b)). Similar performance of the solution scheme could be observed as in the previous case.

6. Conclusion

The methodology for solving the coupled problems in nonlinear mechanics and optimal design of a heterogeneous material was developed and illustrated on a simple example of a model material with two phases, one with behavior described by plasticity and another by damage. We discussed in detail the shape optimization

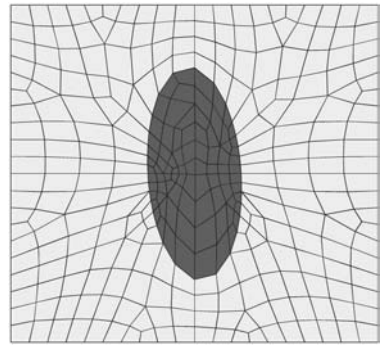

Figure 19.
Shape of inclusions that maximizes plastic dissipation at the constraint imposed on the damage

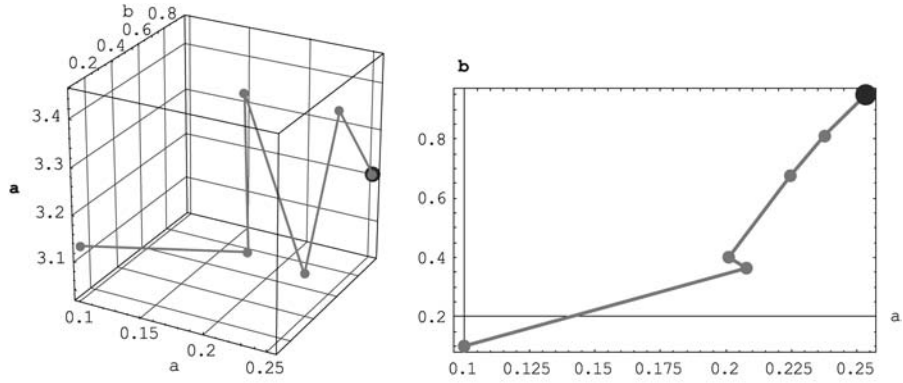

Notes: Projection on the sub-space of half-axes is shown on the right-hand side

Figure 20.
Solution path of the FSQP method to the solution from figure

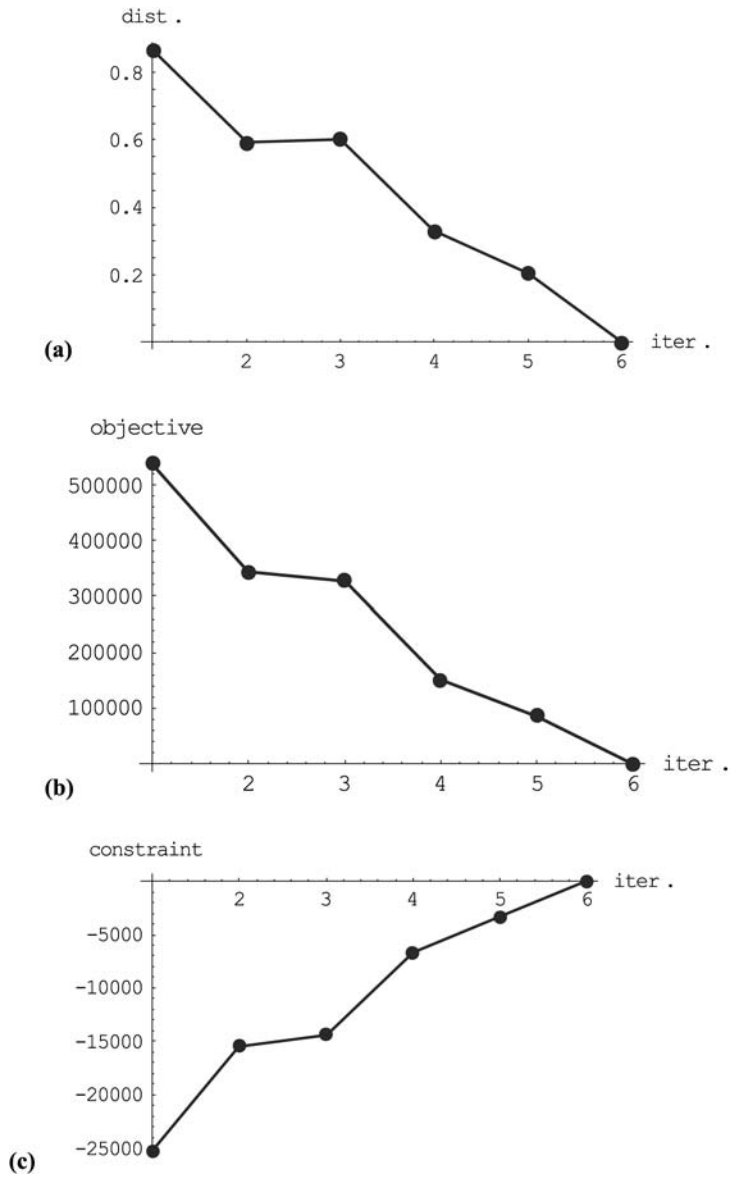

Figure 21.
Course of: (a) distance from the optimum; (b) the objective function; and (c) the constraint through iterations shown in the figure

problem for the internal interface between two phases. The desired optimization goal is defined in terms of the objective and constraint functions, which are related to the micro-scale response of the material under consideration. Furthermore, we considered a periodic microstructure of the material, where each periodic cell consists of a plastic matrix phase into which a single inclusion represented by a damage model is

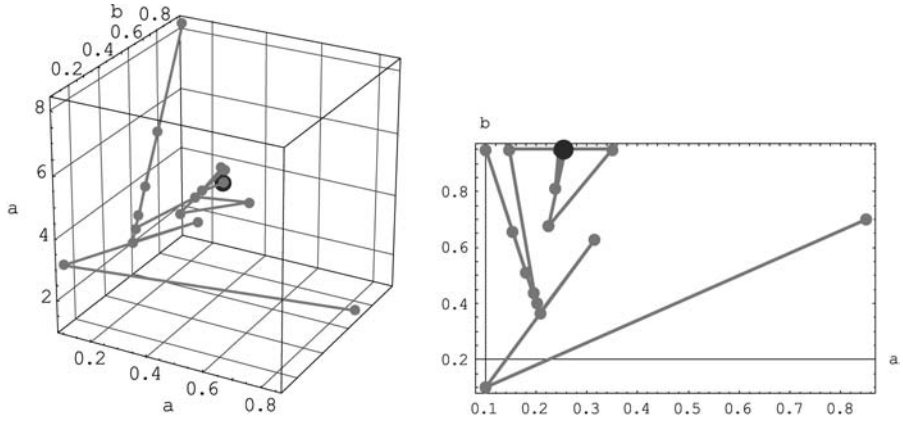

Figure 22.
Solution path from figure, with all evaluation points shown

incorporated. Such geometric layout is in accordance with practicability of production for artificial materials.

We chose elliptical shapes of inclusions. With such a choice, as well as the periodicity of the microstructure and the exact finite element representation of each sub-domain occupied by a single phase within each cell, we manage to reduce drastically the number of design variables to only three. In other words, at each iterative stage of the shape design procedure, we can recover the position of all nodes in the mesh of micro-scale elements from the given current values of the half-axes and the inclination angle of the elliptic interface. Several important benefits are related to chosen interface parameterization. First, the form of the shape transform and number of design parameters restrict the range of achievable shapes, which can be useful for avoiding too complex shapes and regularizing the shape optimization problem. Since the shape transform is defined continuously over the whole domain of the periodic cell, derivatives of the nodal positions are readily available and can be used as input for sensitivity analysis. Finally, the finite element mesh depends smoothly on the design parameters and therefore, the calculated response is less noisy.

We were therefore able to ensure the superior performance of the gradient-based sequential programming optimization algorithm over the non-gradient simplex method, even without using analytic result for sensitivity analysis of the multi-scale model, but only numerical differentiation to compute the gradients. The calculated response was smooth enough to achieve stable convergence of the gradient-based optimization algorithm. On the other hand, the level of noise was high enough that the choice of the right step size for numerical differentiation turned critical. These findings indicate that further effort in the implementation of the sensitivity analysis of the mechanical model would be worthy.

One can imagine a number of possible applications of the presented approach, anywhere from designing the material microstructure which will reduce as much as possible the damage in a given zone, thus increasing the durability of the structure, to designing the material microstructure which will maximize the damage in a given

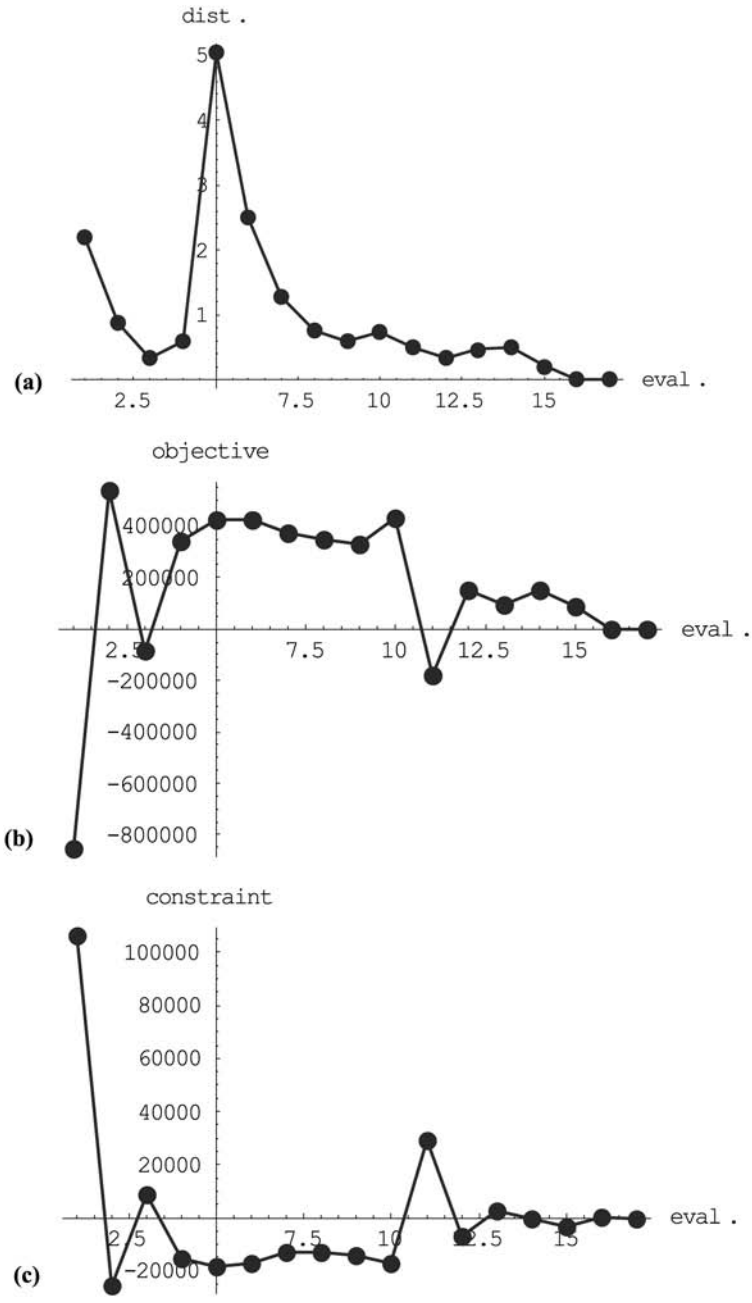

Note: Evaluation number is shown on the horizontal axis, but evaluations performed at alternately perturbed parameters for calculation of parametric derivatives are not included

Figure 23.
Course of: (a) distance from the optimum; (b) the objective function; and (c) the constraint through evaluations shown in the figure

zone, where it is important to concentrate energy dissipation in a structure. The chosen design goals in engineering applications would not only depend on the purpose for which a particular structural element would be used but also on the way how this element is integrated in the whole structure, its interaction with other parts of the structure or external media, and the range of possible loading conditions. The latter may gives rise to additional complexities, such as taking into account multiple loading conditions or simultaneous optimization of internal phase boundary and external shape of the element. We envisage that the solution scheme could be extended in a straightforward way to comply with such requirements. Minor extensions would be needed and also be possible in order to allow for non-periodic microstructure with continuous variation of its shape over macroscopic domain.

One of the most crucial components of the presented approach is parameterization of the interface between the material phases. In the case of a single inclusion incorporated in the surrounded matrix material, the applied parameterization can easily be extended to cover more complex shapes. This may require more robust approach for dealing with mesh distortion, in particular automatic generation of mesh upon the mesh independent definition of the inclusion boundary. Beside the technical difficulties this would inevitably lead to more noisy response functions, and one should consider application of more optimization techniques that are more robust in the presence of noise. In order to allow even more general microstructure of the representative volume, some other technique of defining the interface boundary should be considered, such as the level set method (Wang *et al.*, 2003). Such situation would arise, e.g. when one should account for multiple inclusions of irregular shapes and without defined location within the representative volume. In this case, use of a fixed regular mesh over the complete domain of the micro problem may be worth of consideration, such that material composition and representation of the interface between the matrix and inclusion material would be dealt with at the level of an individual element rather than on the element interface level (Ibrahimbegovic and Markovic, 2003). As the final challenge for the future work in this domain, we see the optimal design of the non-deterministic material structure, where only some probabilistic parameters of the phase distribution can be adjusted.

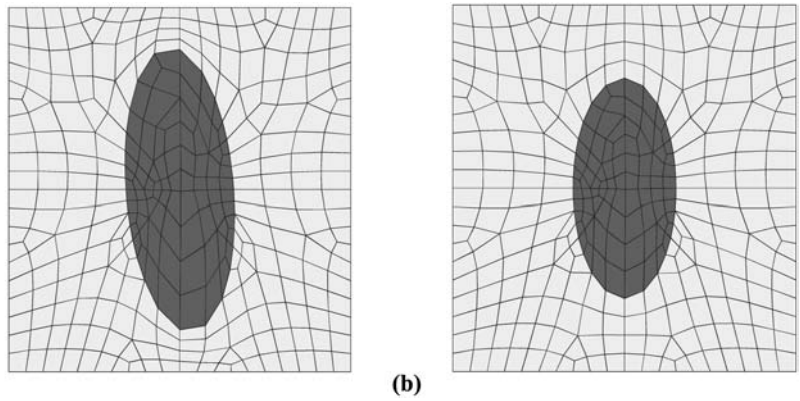

Figure 24.
Optimal shapes of inclusions calculated for: (a) maximization of plastic dissipation with constraint on maximum volume; and (b) minimization of plastic dissipation with constraint on the minimum work of external forces

Note

1. Note that **F** defines a spatial map of the whole periodic cell consistently with the transform of the boundary between the two phases.

References

Bängtsson, E., Noreland, D. and Berggren, M. (2003), "Shape optimization of an acoustic horn", *Comput. Methods. Appl. Mech. Eng.*, Vol. 192 Nos 11/12, pp. 1533-71.

Bonnans, J.F., Panier, E.R., Tits, A.L. and Zhou, J.L. (1992), "Avoiding the Maratos effect by means of a nonmonotone line search. II: inequality constrained problems – feasible iterates", *SIAM J. Numer. Anal.*, Vol. 29, pp. 1187-202.

Dennis, J.E. Jr and Schnabel, R.B. (1996), *Numerical Methods for Unconstrained Optimization and Nonlinear Equations*, SIAM, Philadelphia, PA.

Fletcher, R. (1996), *Practical Methods of Optimization*, 2nd ed., Wiley, New York, NY.

Grešovnik, I. (n.d.), "Quick introduction to optimization shell inverse", available at: www.c3m.si/inverse/doc/ other/

Grešovnik, I. (2000), "A general purpose computational shell for solving inverse and optimisation problems – applications to metal forming processes", PhD thesis, University of Wales Swansea, available at: www.c3m.si/inverse/doc/phd

Grešovnik, I. and Rodič, T. (1999), "A general-purpose shell for solving inverse and optimisation problems in material forming", in COVAS and Antonio, J. (Eds), *Proc. 2nd ESAFORM Conf. on Material Forming*, *Guimaraes*, *Portugal*, pp. 497-500.

Grešovnik, I. and Rodič, T. (2003), "An integral approach to optimization of forming technology", *Proceedings the 5th World Congress of Structural and Multidiscliplinary Optimization*, *Lido di Jesolo*, *Italy*.

Ibrahimbegovic, A. and Knopf-Lenoir, C. (2003), "Shape optimisation of elastic structural systems undergoing large rotations: simultaneous solution procedure", *Computer Model. Eng. Sci.*, Vol. 4, pp. 337-44.

Ibrahimbegovic, A. and Markovic, D. (2003), "Strong coupling methods in multiphase and multiscale modeling of inelastic behavior of heterogeneous structures", *Comput. Meth. Appl. Mech. Eng.*, Vol. 192, pp. 3089-107.

Ibrahimbegovic, A., Markovic, D. and Gatuingt, F. (2003), "Constitutive model of coupled damage-plasticity and its finite element implementation", *Europ. J. Finite Element*, Vol. 12, pp. 381-405.

Ibrahimbegovic, A., Knopf-Lenoir, C., Kucerova, A. and Villon, P. (2004), "Optimal design and optimal control of elastic structures undergoing finite rotations and deformations", *Int. J. Numer. Meth. Eng.*(in press).

Kleiber, M., Autmer, H., Hoen, T.D. and Kowalezyk, P. (1997), *Parameter Sensitivity in Nonlinear Mechanics: Theory and Finite Element Computations*, Wiley, New York, NY.

Lawrence, C.T. and Tits, A.L. (1996), "Nonlinear equality constraints in feasible sequential quadratic programming", *Optimization Methods and Software*, Vol. 6, pp. 265-82.

Lawrence, C.T., Zhou, J.L. and Tits, A.L. (1995), *User's Guide for CFSQP Version 2.3: A C Code for Solving (Large Scale) Constrained Nonlinear (Minimax) Optimization Problems, Generating Iterates Satisfying All Inequality Constraints*, Institute for Systems Research, College Park, MD.

Markovic, D., Ibrahimbegovic, A., Niekamp, R. and Matthies, H. (2004), "Parallelized algorithm for multi-scale modeling of hetergeneous structures with inelastic constitutive behavior", *Proceedings NATO-ARW*, *Bled*, *Slovenia*, *June*.

Markovic, D., Niekamp, R., Ibrahimbegovic, A., Matthies, H. and Taylor, R.L. (n.d.), "Multi-scale modeling of heterogeneous structures with inelastic constitutive behavior. Part I: Physical and mathematical aspects", *Eng. Computing*, Vol. 22 Nos 5/6.

Melnyk, S. (2004), "Shape optimization of inclusion in a heterogeneous material", MSc thesis, ENS-Cachan (in French).

Panier, E. and Tits, A.L. (1993), "On combining feasibility, descent and superlinear convergence in inequality constrained optimization", *Mathematical Programming*, Vol. 59, pp. 261-76.

Pian, T.H.H. and Sumihara, K. (1984), "Rational approach for assumed stress finite elements", *Int. J. Numer. Meth. Eng.*, Vol. 20, pp. 1638-85.

Rodič, T. and Gresovnik, I. (1998), "A computer system for solving inverse and optimization problems", *Eng. Computer*, Vol. 15 No. 7, pp. 893-907.

Taylor, R.L. (2004), *FEAP: Finite Element Analysis Program – User's Manual*, available at: www.uc.ce.edu/rtl

Tortorelli, D.A. and Michaleris, P. (1994), "Design sensitivity analysis: overview and review", *Inverse Prob. Eng.*, Vol. 1, pp. 71-105.

Tsay, J.J. and Arora, J.S. (1990), "Nonlinear structural design sensitivity analysis for path dependent problems. Part i and ii", *Comput. Meth. Appl. Mech. Eng.*, Vol. 81, pp. 183-228.

Wang, M.Y., Wang, X. and Guo, D. (2003), "A level set method for structural topology optimization", *Comput. Methods. Appl. Mech. Eng.*, Vol. 192, pp. 227-46.

Wriggers, P. and Zohdi, T.I. (2001), "Computational testing of new materials", *Proceedings ECCM 2001*, Crackow, Poland.

Appendix. Coupled non-linear mechanics-optimisation problem in 1D setting

In order to clarify the ideas presented in the main body of the paper, we provide in this Appendix a more detailed presentation of the coupled nonlinear mechanics-optimization problem in a simple 1D setting. In order to have the same ingredients as in the original problem, we chose the simplest possible case where one macroscale truss-bar element consists of two micro-scale bar elements, one with constitutive behaviour described by plastic and another by damage model (see Figure A1).

The behavior of the plastic component is described by the classical hardening plasticity model (Ibrahimbegovic *et al.*, 2003) with three fundamental ingredients of the additive decomposition of strain, strain energy function and the yield criterion

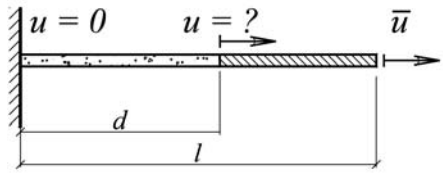

$$\Omega_d = [0,d], \qquad \Omega = [0,l]$$
$$\Omega_p = [d,l], \qquad \Omega = \Omega_d \cup \Omega_p$$

Figure A1.

Note: Model problem of a bar: one macroscale element represented by two micro-scale truss-bar elements, one with damage and the other with plastic behavior

$$\varepsilon = \varepsilon^e + \varepsilon^p$$

$$\Psi^p(\varepsilon, \varepsilon^p, \xi^p) = \frac{1}{2}(\varepsilon - \varepsilon^p)E(\varepsilon - \varepsilon^p) + \frac{1}{2}K^p(\xi^p)^2 \tag{A1}$$

$$\Phi^p(\sigma, q^p) = |\sigma| - (\sigma_y - q^p) \leq 0$$

The remaining equations of the model on constitutive relations for stress and evolution equations for internal variables can be obtained from standard thermodynamics developments and principle of maximum plastic dissipation with

$$\sigma = \frac{\partial \Psi^p}{\partial \varepsilon} = E(\varepsilon - \varepsilon^p); \qquad q^p = -\frac{\partial \Psi^p}{\partial \xi^p} = -K^p \xi^p$$

$$\dot{\varepsilon}^p = \dot{\gamma}^p \frac{\partial \Phi^p}{\partial \sigma} = \dot{\gamma}^p \operatorname{sgn}(\sigma^p); \qquad \dot{\xi}^p = \dot{\gamma}^p \frac{\partial \Phi^p}{\partial q^p} = \dot{\gamma}^p \tag{A2}$$

Similarly, the fundamental ingredients of damage model are the choice of compliance in order to describe the damage, the strain energy and the damage criterion:

$$\chi^d = \frac{1}{2}\sigma D \sigma$$

$$\psi^d(\varepsilon, D, \xi^d) = \sigma\varepsilon - \chi^d + \frac{1}{2}K^d(\xi^d)^2 \tag{A3}$$

$$\Phi^d(\sigma, q^d) = |\sigma| - (\sigma_f - q^d) \leq 0$$

The remaining ingredients of constitutive and evolution equations are again obtained from thermodynamics and the principle of maximum damage dissipation:

$$\sigma = \frac{\partial \Psi^d}{\partial \varepsilon} = D^{-1}\varepsilon; \qquad q^d = -\frac{\partial \Psi^d}{\partial \xi^d} = -K^d \xi^d$$

$$\dot{D}\sigma = \dot{\gamma}^d \frac{\partial \Phi^d}{\partial \sigma} = \dot{\gamma}^d \operatorname{sgn}(\sigma^d); \qquad \dot{\xi}^d = \dot{\gamma}^d \frac{\partial \Phi^d}{\partial q^d} = \dot{\gamma}^d \tag{A4}$$

The equilibrium equations in the present case, with macroscale displacement field already known given as 0 and $\bar{u}$ (Figure A1), reduce to a set of equilibrium equations with unknown displacements at the micro-scale. For the mesh consisting of the elements with exact microstructure representation, where the first element covers the domain Ω_d and the second element covers the domain Ω_p, the only unknown displacement at the micro-scale is the displacement at the interface, u (Figure A1). The weak form of the equilibrium equations at the micro-scale can then be written as

$$G_u(u, V; w) = \int_{\Omega^p} \frac{\mathrm{d}w}{\mathrm{d}x}\sigma(u, \varepsilon^p, \xi^p, \bar{u})\,\mathrm{d}x + \int_{\Omega^d} \frac{\mathrm{d}w}{\mathrm{d}x}\sigma(u, D, \xi^d)\,\mathrm{d}x = 0, \tag{A5}$$

where

$$V = (\varepsilon^p, \xi^p, D, \xi^d, \dot{\varepsilon}^p, \dot{\xi}^p, \dot{D}, \dot{\xi}^d, \dot{\gamma}^p, \dot{\gamma}^d) \tag{A6}$$

There is a single design variable describing the interface position d between the plastic and the damage bars. The coupled non-linear mechanical-optimisation problem of this kind can then be rewritten as

$$\min_{d,u,V} \max_{\lambda} L(d,u,V;\lambda); \quad L(d,u,V;\lambda) = J(d,u,V) + G(d,u,V;\lambda), \tag{A7}$$

where

$$\lambda_a = \{\lambda^{eq}, \lambda^{\Phi^p}, \lambda^{\Phi^d}, \lambda^{\varepsilon^p}, \lambda^{\xi^p}, \lambda^{D}, \lambda^{\xi^d}\} \tag{A8}$$

are the Lagrange multipliers enforcing the constraints imposed by different mechanical equations.

For clarity we can also write an explicit form of the last term in equation (A7) for the chosen model problem given as

$$G(d,u,V;\lambda) = \left\{ \begin{array}{c} \int_{\Omega^p} \frac{\partial \lambda^{eq}}{\partial x} \sigma(d,u,\varepsilon^p,\xi^p,\dot{\lambda}^p)\,\mathrm{d}x + \int_{\Omega^d} \frac{\partial \lambda^{eq}}{\partial x} \sigma(d,u,D,\xi^d,\dot{\gamma}^d)\,\mathrm{d}x \\ [\Phi^p(\sigma,q^p)\cdot\dot{\gamma}^p]\lambda^{\Phi^p} \\ [\dot{\varepsilon}^p - \dot{\gamma}^p \mathrm{sgn}(\sigma^p)]\lambda^{\varepsilon^p} \\ [\dot{\xi}^p - \dot{\gamma}^p]\lambda^{\xi^p} \\ [\Phi^d(\sigma,q^d)\cdot\dot{\gamma}^d]\lambda^{\Phi^d} \\ [\dot{D}\sigma - \dot{\gamma}^d \mathrm{sgn}(\sigma^d)]\lambda^{D} \\ [\dot{\xi}^d - \dot{\gamma}^d]\lambda^{\xi^d} \end{array} \right\}. \tag{A9}$$

We note that only the first of these equations is global in the sense that it concerns the whole domain $\Omega = \Omega_p \cup \Omega_d$ whereas the others are local equations which concern only a given quadrature point.

The only ingredient which remains to specify is the cost function, corresponding to the first term in equation (A7). An explicit form of the cost function in equation (A7) above can be written in accordance with a given goal; one possible choice advocated in this paper is related to the dissipation, which can be written for damage D^d and plastic component D^p as

$$D^d(d,u,D,\xi^d,\dot{\gamma}^d) = \frac{1}{2}\sigma\dot{D}\sigma + q^d\dot{\xi}^d; \quad D^p(d,u,\varepsilon^p,\xi^p,\dot{\gamma}^p) = \sigma\dot{\varepsilon}^p + q^p\dot{\xi}^p \tag{A10}$$

Such a choice would clearly involve all the variables and would allow for any preference in the solution procedure. An analytic solution of this problem can be provided in several cases (Melnyk, 2004), which is very useful for testing various phases of software development.

In a more general case where the analytic solution is not available, one has to compute the solution numerically. One can start by first solving the equilibrium equation and computing the evolution of the internal variables, which can be written as

$$0 = \frac{\partial L}{\partial \lambda} = G \Rightarrow (u, \varepsilon^p, \xi^p, \dot{\gamma}^p, D, \xi^d, \dot{\gamma}^d) \tag{A11}$$

We indicated in equation (A11) that this first step allows us to compute all the values of the mechanical state variables. The next step is the computation of the Lagrange multipliers according to

$$0 = \frac{\partial L}{\partial V} = \frac{\partial J}{\partial V} + \lambda^V \frac{\partial G}{\partial V}; \quad 0 = \frac{\partial L}{\partial u} = \frac{\partial J}{\partial u} + \lambda^{eq} \frac{\partial G}{\partial u}. \tag{A12}$$

The latter defines a linear problem as the consequence of the dual formulation we adopted herein. Moreover, the solution is already well prepared by the previous computational stage in equation (A11), where, for example, the last equation would simply call for the tangent matrix K to obtain

$$K\lambda^{eq} = -\frac{\partial J}{\partial u}; \quad K = -\frac{\partial G}{\partial u} \tag{A13}$$

Having computed the solution for the Lagrange multipliers we can then proceed to computing the values of the design variables according to

$$0 = \frac{\partial L}{\partial d} = \frac{\partial J}{\partial d} + \lambda \frac{\partial G}{\partial d} \tag{A14}$$

For example, for a given choice of the cost function $[J - J_0]^2$, we can write an explicit form (Melnyk, 2004) of this equation as

$$\begin{aligned}
&\sum_{n=1}^{n_{\text{inc}}} \sum_{\alpha=1}^{npg} \Bigg\{ \left[\left[J_{\alpha,n}^{d} - J_0 \right]^2 w_{\alpha,n} - \left[J_{\alpha,n}^{p} - J_0 \right]^2 w_{\alpha,n} + \frac{\partial \lambda_{\alpha,n}^{eq,d}}{\partial x} \sigma_{\alpha,n} w_{\alpha,n} - \frac{\partial \lambda_{\alpha,n}^{eq,p}}{\partial x} \sigma_{\alpha,n} w_{\alpha,n} \right] \cdot d^2 \\
&- \left[\left[J_{\alpha,n}^{d} - J_0 \right]^2 w_{\alpha,n} - \left[J_{\alpha,n}^{p} - J_0 \right]^2 w_{\alpha,n} + \frac{\partial \lambda_{\alpha,n}^{eq,d}}{\partial x} \sigma_{\alpha,n} w_{\alpha,n} - \frac{\partial \lambda_{\alpha,n}^{eq,p}}{\partial x} \sigma_{\alpha,n} w_{\alpha,n} \right] \cdot l \cdot d \\
&+ [J_{\alpha,n} - J_0] \dot{\lambda}_{\alpha,n}^{d} \operatorname{sgn}\left(\sigma_{\alpha,n}^{d} \right) \left(D_{\alpha,n}^{-1} \right) \left(-\sum_{b=1}^{2} (-1)^b u_b^e \right) w_{\alpha,n} d - 2[J_{\alpha,n} - J_0] \dot{\varepsilon}_{\alpha,n}^{p} C \\
&\times \sum_{b=1}^{2} (-1)^b u_b^e w_{\alpha,n} d + \frac{\partial \lambda_{\alpha,n}^{eq,d}}{\partial x} \left(D_{\alpha,n}^{-1} \right) \left(-\sum_{b=1}^{2} (-1)^b u_b^e \right) w_{\alpha,n} d - \frac{\partial \lambda_{\alpha,n}^{eq,p}}{\partial x} C \sum_{b=1}^{2} (-1)^b u_b^e w_{\alpha,n} d \\
&- \lambda_{\alpha,n}^{\Phi^p} \dot{\gamma}_{\alpha,n}^{p} \operatorname{sgn}\left(\sigma_{\alpha,n}^{p} \right) C \sum_{b=1}^{2} (-1)^b u_b^e w_{\alpha,n} d + \lambda_{\alpha,n}^{\Phi^d} \dot{\gamma}_{\alpha,n}^{d} \operatorname{sgn}\left(\sigma_{\alpha,n}^{d} \right) \left(D_{\alpha,n}^{-1} \right) \\
&\times \left(-\sum_{b=1}^{2} (-1)^b u_b^e \right) w_{\alpha,n} d + \lambda_{\alpha,n}^{D} \dot{D}_{\alpha,n} \left(D_{\alpha,n}^{-1} \right) \left(-\sum_{b=1}^{2} (-1)^b u_b^e \right) w_{\alpha,n} d \\
&- [J_{\alpha,n} - J_0] \dot{\gamma}_{\alpha,n}^{d} \operatorname{sgn}\left(\sigma_{\alpha,n}^{d} \right) \left(D_{\alpha,n}^{-1} \right) \left(-\sum_{b=1}^{2} (-1)^b u_b^e \right) w_{\alpha,n} \cdot l \\
&+ \frac{\partial \lambda_{\alpha,n}^{eq,d}}{\partial x} \left(D_{\alpha,n}^{-1} \right) \sum_{b=1}^{2} (-1)^b u_b^e w_{\alpha,n} \cdot l - \lambda_{\alpha,n}^{\Phi^d} \dot{\gamma}_{\alpha,n}^{d} \operatorname{sgn}\left(\sigma_{\alpha,n}^{d} \right) \left(D_{\alpha,n}^{-1} \right) \left(-\sum_{b=1}^{2} (-1)^b u_b^e \right) w_{\alpha,n} \cdot l \\
&- \lambda_{\alpha,n}^{D} \dot{D}_{\alpha,n} \left(D_{\alpha,n}^{-1} \right) \left(-\sum_{b=1}^{2} (-1)^b u_b^e \right) w_{\alpha,n} \cdot l \Bigg\} = 0
\end{aligned} \tag{A15}$$

By computing the value of d we complete one computational cycle. Similarly, one can complete as many cycles as needed in order to obtain the solution for any particular choice of the cost function.